Nonlinear Differential Games-Based Impact-Angle-Constrained Guidance Law

Rajarshi Bardhan* and Debasish Ghose†
Indian Institute of Science, Bangalore 560 012, India

DOI: 10.2514/1.G000940

The problem of intercepting a maneuvering target at a prespecified impact angle is posed in nonlinear zero-sum differential games framework. A feedback form solution is proposed by extending state-dependent Riccati equation method to nonlinear zero-sum differential games. An analytic solution is obtained for the state-dependent Riccati equation corresponding to the impact-angle-constrained guidance problem. The impact-angle-constrained guidance law is derived using the states line-of-sight rate and projected terminal impact angle error. Local asymptotic stability conditions for the closed-loop system corresponding to these states are studied. Time-to-go estimation is not explicitly required to derive and implement the proposed guidance law. Performance of the proposed guidance law is validated using two-dimensional simulation of the relative nonlinear kinematics as well as a thrust-driven realistic interceptor model.

Nomenclature

a_I	=	lateral acceleration of the interceptor, m/s^2
a_T	=	lateral acceleration of the target, m/s^2
$\mathcal{C}^1$	=	set of continuously differentiable functions
D	=	drag, N
D_i	=	induced drag, N
D_0	=	zero-lift drag, N
g	=	acceleration due to gravity, m/s^2
$\mathcal{H}$	=	Hamiltonian of the game
$\mathbf{H}$	=	Hamiltonian matrix
$\mathbf{I}_j$	=	identity matrix of dimension j
J	=	objective functional of the related game
M	=	Mach number
m_I	=	mass of the interceptor, kg
n	=	number of states
n_e	=	number of controls of the evader/target
n_p	=	number of controls of the pursuer/interceptor
$\mathbf{Q}$	=	state weighting matrix
$\mathbb{R}^l$	=	l-dimensional vector space over real number field $\mathbb{R}$
$\mathbf{R}_1$	=	pursuer's control weighting matrix
$\mathbf{R}_2$	=	evader's control weighting matrix
r	=	distance of the target from the interceptor, m
T_I	=	interceptor's thrust, N
u	=	commanded lateral acceleration by the interceptor, m/s^2
$\boldsymbol{u}$	=	pursuer's control vector
V_I	=	velocity of the interceptor, m/s
V_T	=	velocity of the target, m/s
v	=	commanded lateral acceleration by target, m/s^2
$\boldsymbol{v}$	=	evader's control vector
$\boldsymbol{x}$	=	state vector
x_I	=	x coordinate of interceptor's position, m
x_T	=	x coordinate of target's position, m
z_I	=	z coordinate of interceptor's position, m
z_T	=	z coordinate of target's position, m
α	=	flight-path angle of the interceptor, rad
β	=	flight-path angle of the target, rad
$\boldsymbol{\lambda}$	=	vector of costates
η	=	projected terminal impact angle, rad
η^C	=	desired impact angle, rad
θ	=	angle subtended by the line-of-sight to the reference frame, rad
σ	=	line-of-sight rate, rad/s
$\mathbf{0}_{i\times j}$	=	matrix with i rows and j columns with all elements equal to zero

Received 1 August 2014; revision received 6 November 2014; accepted for publication 7 November 2014; published online 5 February 2015.

*Student, Department of Aerospace Engineering.
†Professor, Department of Aerospace Engineering.

I. Introduction

LETHALITY of warheads against targets is enhanced at specific impact angles while intercepting a target. Also, if the target employs countermeasures, which are effective in limited range and azimuthal zone, then controlling the interceptor impact angle can be an effective means of avoiding such countermeasures. A growing volume of literature in recent years marks the importance of impact-angle-constrained guidance.

Proportional navigation-based guidance (PNG) laws and its variants have been used to solve impact-angle control problems. The problem of achieving all impact angles against a stationary target was addressed in [1] following an idea of a two-stage PNG law. This guidance law consists of an initial orientation phase where a navigation constant of value less than 2 is used depending on the initial engagement geometry and the desired impact angle, followed by a switch over to a guidance phase where a navigation constant of value greater than or equal to 2 is used to achieve the impact angle. The same idea was later extended for impact-angle control guidance against moving but nonmaneuvering targets in [2]. A guidance law that provides the desired interception angle against a stationary or slowly moving target was derived in [3] with combination of PNG and a feedback of the difference between the desired interception angle and the predicted interception angle using PNG. In [4], a modified PNG law, with a time-varying bias component added to the line-of-sight (LOS) rate, was proposed against a moving nonmaneuvering target to impose a specified impact angle. By means of simulation, this guidance law was shown to exhibit good performance against slowly maneuvering targets. Two-phase guidance-scheme-based biased proportional navigation guidance laws were proposed in [5,6] for impact-angle control against stationary targets. Both of these guidance laws use only the LOS rate information. A constant bias was used in [5], whereas Kim et al. [6] used two time-varying biases and took into account both the terminal-angle constraint and look-angle limitation to maintain the seeker lock-on condition. An adaptive guidance approach in a proportional navigation form was proposed in [7] that considered an aerodynamic model of an interceptor for terminal intercept-angle constraint problem against a stationary target. In [8], a passive guidance law that requires LOS and LOS rate information but does not depend on range was proposed to achieve a desired impact angle against a stationary or slow-moving surface target. However, these guidance laws proposed

in [1–8] were not designed considering targets with high maneuver capabilities.

A guidance law called circular navigation guidance was proposed in [9] that enables a missile to intercept a nonmaneuvering target at the desired impact angle following a circular arc path. This guidance law cannot be applied against targets maneuvering with high magnitudes.

Based on linearized kinematics, guidance laws were derived using linear optimal control theory for impact-angle control problems. In [10], an optimal guidance law was formulated by minimizing a quadratic cost function involving impact-angle error and miss distance for an engagement between a reentry vehicle and a fixed or slow-moving ground target. An optimal guidance law was proposed in [11] for impact-angle control of an interceptor against a ship maneuvering with a constant low magnitude and under the assumption of a small initial heading error. Integrating a suboptimal estimation filter was necessary to estimate different parameters and relative states, which were required by the guidance law in [11]. In [12], optimal control laws were derived for lag-free and first-order lag missile systems to intercept a stationary target at a desired impact angle by optimizing a cost functional involving total control effort and penalty terms on terminal states. In the same settings, Ryoo et al. [13] used a time-to-go weighted energy cost function to shape an interceptor's trajectory. A guidance law, called generalized explicit guidance law, based on linear optimal control theory and simple linearized engagement kinematics, was proposed in [14] both for two-dimensional and three-dimensional (3-D) engagement to achieve design specifications on miss distance and final missile-target relative orientation. The control usage and thus degree of curvature in the trajectory were determined by a design coefficient that needed to be preselected. Analytic solutions of a generalized impact-angle-control guidance law for a first-order lag system were investigated in [15] to scrutinize the effects of system lag on a first-order missile system under the assumptions of a stationary or slow-moving target. These analytical solutions gave insight into how system lag and guidance coefficients affect terminal misses. Planar optimal control-based interception laws against maneuvering targets with known trajectories and constraints on initial and final flight-path angles of the interceptor were presented in [16]. Linear quadratic optimal (OGL-CTIA) and differential games guidance laws (LQDG-CTIA), which enable interceptors to impose prespecified terminal intercept angles to maneuvering targets, were presented in [17] based on linearized models. Both the guidance laws performed well by providing near-zero values of miss distance and intercept-angle error against different kinds of target maneuvers in the simulations. OGL-CTIA requires the target's maneuver information, whereas LQDG-CTIA does not. A closed-form guidance scheme was proposed in [18] for a missile with time-varying acceleration constraint to satisfy a terminal impact-angle constraint. The guidance law was formulated for a maneuvering target based on linear quadratic optimal control theory. The time-varying guidance gains, required to compute a feedback-type command, were obtained from an iterative numerical procedure. The concept of zero-effort collision triangle was introduced in [19], and an impact-angle control optimal guidance law was developed for missiles with arbitrary velocity profiles against maneuvering targets based on the linearization of kinematics around the zero-effort collision triangle. The guidance laws derived in [10–15] did not consider maneuvering targets in their formulations. Although maneuvering targets are considered in the optimal guidance laws derived in [16–19], the target's trajectory needs to be known [16], or the target's maneuver profile is required to be exactly known [17,18], or it is assumed that the target position and velocity are known and its future maneuver can be predicted without error [19].

An issue related to the implementation of the guidance laws that are derived from linearized kinematics is the assumption of availability of a precise time-to-go estimate. Sensitivity analysis of optimal control-based guidance laws toward time-to-go estimation error shows that error in estimation of this quantity may lead to degradation of performance [20,21]. However, with the exceptions of [12,13], no such sensitivity analysis exists for the optimal guidance laws derived in [10,11,14–19] or for LQDG-CTIA derived in [17], which are related to impact-angle control problems. When an interceptor starts on the collision course or with a slight deviation from it, then time-to-go calculated as the ratio of range to closing velocity provides a good estimate of time-to-go. However, as observed in [12], this method does not take into account curvature of the trajectory required for the impact-angle control. Therefore, this method of estimating time-to-go does not reflect the effect of the terminal impact-angle constraint on time-to-go. It was suggested in [17] to use time-to-go estimate, as given in [12], when deviation from the collision course is large. But in [12], time-to-go estimate for an impact-angle-constrained optimal guidance law was derived assuming a stationary or slow-moving target; hence, those time-to-go estimates cannot be used against maneuvering targets. In [19], it was also pointed out that the missile trajectory may largely deviate from the collision triangle to satisfy the specific impact-angle requirement. Hence, the assumption that an interceptor remains close to the collision course in deriving linearized kinematics-based guidance laws may not remain valid when a specific impact angle between the missile and target velocity vectors is required. Thus, a guidance law that is independent of time-to-go estimate, and which is not derived from linearized kinematics based on near-collision course engagement geometry assumption, is more desired for impact-angle control against a maneuvering target. This is the primary motivation behind the present paper.

Nonlinear optimal control-based guidance laws have also been used in impact-angle-constrained guidance problems. These guidance laws are expected to perform well even when the engagement trajectory has large deviation from the collision course because linearized kinematics are not assumed in their derivations. A guidance algorithm was derived from a direct method of calculus of variations for trajectory shaping and to meet several terminal constraints in [22]. The final form of the trajectory optimization problem was a nonlinear programming problem in a number of parameters, which is solved numerically. This algorithm allows combining different criteria into a single weighted compound performance index, but the iterations required for the nonlinear optimization steps may be quite demanding on an onboard processor. The problem of impact-angle-constrained guidance against a stationary target was treated as a nonlinear regulator problem and solved using the state-dependent Riccati equation (SDRE) technique in [23]. Starting with different firing angles, this guidance law was shown to achieve its goals in finite time using the state weights as functions of time-to-go. A nonlinear optimal guidance law was derived in [24] to intercept a stationary target at the designated time and angle while minimizing integral square control effort. A two-point boundary-value problem was solved using a shooting method to obtain values of some parameters that were required to compute the guidance command. Two nonlinear suboptimal midcourse 3-D guidance laws, based on the model predictive static programming (MPSP) method and a closely related model predictive spread control concept [25], were presented in [26] to enforce desired alignment constraints in both elevation and azimuth in a hard-constraint sense against incoming high-speed ballistic missiles. Guidance laws based on MPSP and its variant were presented in [27,28], respectively, for solving a finite-horizon nonlinear optimal control problem with hard terminal constraints and were applied to an impact-angle-constrained problem against a stationary or slow-moving ground target. Simulation results in [27,28] showed that this guidance law performs well against slow-moving targets with low levels of maneuver. MPSP technique depends on a guess control history and an iterative process for update of control to generate a trajectory with desired terminal constraints. With improper choice of guess control history, this technique may take a large number of iterations to converge to the optimal solution. A near-optimal spatial midcourse guidance to a predicted intercept point (PIP) under a terminal angular constraint was presented in [29]. Numerical solutions were presented to the nonlinear problem that includes an aerodynamic model for minimizing the total squared acceleration and for maximizing the total energy at the PIP. The guidance laws derived in [22–24,26,29] do not take into account the target's maneuver in their formulations,

whereas the guidance laws developed in [27,28] depend on information on the target's maneuver.

Sliding-mode control (SMC) theory provides a robust control method that can handle nonlinearity in system states, large modeling errors, and uncertainties. A guidance law based on SMC approach was presented in [30], which can be applied in head-on, tail-chase, and head-pursuit engagement scenarios relative to a maneuvering target's flight direction. Analytical conditions for the existence of these different engagement geometries were also discussed. This guidance law requires estimation of target's maneuver to implement the equivalent control law. While deriving the proposed guidance law, a "near collision course" assumption was not made, which makes the guidance law applicable both in the midcourse and endgame phases. Finite-time convergent guidance laws to intercept stationary, constant velocity, and maneuvering targets at desired impact angles were presented in [31] based on sliding mode control theory. The problem of singularity at the terminal instant in [31] was later removed in [32] using nonsingular terminal sliding mode control theory. The proposed guidance law in [32] was shown to impose desired impact angles with negligible miss distance. Though target's maneuver information is required to implement the equivalent control law derived in [32], robustness of the guidance law against a maneuvering target was shown by presenting simulation results for a case where the target's maneuver information was not assumed to be known. An impact-angle-constrained guidance law against a maneuvering target using partial integrated guidance and control logic was proposed in [33] with the desired impact angle defined along a prespecified LOS direction. A continuous sliding-mode control law was designed in this work, integrating continuous saturation function in the controller to stabilize a class of uncertain nonlinear systems. Though sliding mode controllers are robust with respect to uncertainties, most of these controllers are discontinuous due to the use of the signum function, which may demand high rates of control. Chattering is another difficulty during implementation of these guidance laws. Use of the boundary-layer approach to remove chattering may lead to a compromise on robustness. Moreover, a guidance law derived from sliding mode control theory does not cater to optimizing a cost functional like total control effort over the engagement period.

Performance of optimal control-based guidance laws against maneuvering targets [16–19,27,28] depends on how exact the available information on target maneuver is. But the assumption on the availability of exact information about a target's maneuver is very strict because the future course of action of the target, an independent entity, cannot be predicted beforehand. SMC-based guidance laws designed for impact-angle control need the target's acceleration to be known in the equivalent control components [30–32]. In the absence of any information on target maneuver, SMC-based guidance laws may perform well if the magnitude of the target's acceleration and its rate of variation remain within certain bounds. On the other hand, differential games-based guidance laws do not need accurate information about a target's maneuver because they are designed to withstand the worst-case maneuver of the target. In this work, the problem of intercepting a maneuvering target at a specified intercept angle is formulated as a pursuer–evader nonlinear zero-sum differential game to obtain a guidance law that can intercept a maneuvering target at a given impact angle, even without having any information about the target's maneuver, and can perform robustly even when the engagement geometry is not close to the collision course. It has been already discussed that independence from the information requirement about an adversary's strategy is a characteristic of the strategies derived from zero-sum differential games. To meet the second desired criterion, the guidance law needs to be derived without linearizing or making any such assumptions on the dynamics of the required states. The terms "pursuer" and "interceptor" are interchangeably used throughout the text as well as the terms "evader" and "target". It was indicated in [17] that if the initial geometry has a large deviation from the collision course, then they use SDRE method by linearizing the equations of motion at each time step and then solve the associated SDRE. However, no details were provided there. The idea of using SDRE method to differential games to intercept a target at a specified impact angle was first introduced in [34]. The Hamilton–Jacobi–Bellman–Isaacs (HJBI) equation, the nonlinear partial differential equation that needs to be solved to obtain the saddle-point strategies of a differential game, is unlikely to yield any closed-form analytic solution in the nonlinear multivariable case. Though there are different numerical methods for approximate solutions, these methods may take several iterations to reach a solution at each time step and may be computationally complex [35]. Thus, these methods are hardly implementable online, where solutions are required to be computed fast, like interceptor–target engagement problems. On the other hand, well-developed theory and computational tools for the Riccati equation [36] can be used to obtain solutions to SDRE. The SDRE technique provides an online implementable simple alternative to solving the Hamilton–Jacobi–Bellman (HJB) equation arising in nonlinear regulator problems [37]. A survey on SDRE design methodology and its applications can be found in [37]. It is an effective design technique for synthesizing feedback control in nonlinear regulator problems in the presence of nonlinearities in the system states and offers design flexibility through state-dependent weighting matrices. Apart from the work in [23], SDRE method found its applications in other interceptor–target engagement problems [38–41]. Instead of solving the HJBI associated with the differential game formulation of the impact-angle constraint problem, the present paper extends the idea of SDRE method to obtain an online implementable feedback form solution for the guidance problem. An analytic solution of the SDRE corresponding to an admissible state-dependent coefficient form of the underlying impact-angle control system is derived in this paper. This simplifies online implementation of the derived guidance law because it is no longer required to solve the SDRE at each time step. It should be mentioned here that the guidance law obtained from the derived analytic solution of the SDRE is not the exact saddle-point solution, and hence it is suboptimal in nature. In the derivation of the guidance law, the interceptor and the target are assumed to have constant speeds. In practical scenarios, the speed of the interceptor may not remain constant throughout the engagement duration. Thus, the performance of the guidance law is also studied using a realistic model of an interceptor against a maneuvering target. It is also tested for the cases when initial engagement geometries have large deviations from the collision courses.

The paper is organized as follows. In Sec. II, a general solution to nonlinear pursuer–evader differential games using the SDRE method is presented. The guidance law for the terminal impact-angle-constrained engagement problem is derived in Sec. III according to the proposed framework. Section IV presents performance studies of the developed guidance law based on the simulation results. Section V concludes the paper with a summary of the main results and a discussion on future scope for research.

II. State-Dependent Riccati Equation Design Technique for Differential Games

Consider a pursuer–evader game between a pursuer $\mathcal{P}$ and an evader $\mathcal{E}$ starting at time t_0. The game ends in favor of $\mathcal{P}$ if certain states or parameters related to the engagement satisfy certain criteria defined by a set $\mathcal{B}$. To reach the set $\mathcal{B}$ or win, $\mathcal{P}$ chooses its control vector $\boldsymbol{u}$ to regulate certain states to zero while minimizing its total control effort consumption over the duration of the game. On the other hand, $\mathcal{E}$ has to choose its controls $\boldsymbol{v}$ to steer those states away from zero to evade while minimizing its own total control effort. These two opposite objectives of the two noncooperating players can be incorporated in a single objective function. The objective function is assumed to be of the following form:

$$J = \frac{1}{2}\int_{t_0}^{\infty} (\boldsymbol{x}^T\mathbf{Q}(\boldsymbol{x})\boldsymbol{x} + \boldsymbol{u}^T\mathbf{R}_1(\boldsymbol{x})\boldsymbol{u} - \gamma^2\boldsymbol{v}^T\mathbf{R}_2(\boldsymbol{x})\boldsymbol{v})\,\mathrm{d}t \qquad (1)$$

The objective of $\mathcal{P}$ is to minimize J, whereas the objective of $\mathcal{E}$ is to maximize J in Eq. (1). Note that the objective function contains state-dependent weights.

The state equations evolve as follows:

$$\dot{\boldsymbol{x}} = \mathbf{f}(\boldsymbol{x}) + \mathbf{B}(\boldsymbol{x})\boldsymbol{u} + \mathbf{C}(\boldsymbol{x})\boldsymbol{v}, \qquad \boldsymbol{x}(t_0) = \boldsymbol{x}_0 \tag{2}$$

In Eqs. (1) and (2), $\boldsymbol{x} \in \mathbb{R}^n$ is the state vector, and $\boldsymbol{u} \in \mathbb{R}^{n_p}$ and $\boldsymbol{v} \in \mathbb{R}^{n_e}$ are control vectors of $\mathcal{P}$ and $\mathcal{E}$, respectively. $\mathbf{Q}(\cdot) \in \mathbb{R}^{n\times n}$ is state weighting matrix and has to remain positive semidefinite for all $\boldsymbol{x}$. It is a design parameter as well. The control weight matrices $\mathbf{R}_1(\cdot) \in \mathbb{R}^{n_p\times n_p}$ and $\mathbf{R}_2(\cdot) \in \mathbb{R}^{n_e\times n_e}$ have to remain positive-definite for all $\boldsymbol{x}$.

In Eq. (1), $\gamma > 0$ is a measure of $\mathcal{P}$'s maneuvering capability relative to that of $\mathcal{E}$. The higher the value of γ is, the lower the maneuvering capability of $\mathcal{E}$ is. Selection of γ should be based on the maneuvering capability of the target.

Controls $\boldsymbol{u}$ and $\boldsymbol{v}$ are assumed to remain bounded in $\mathcal{L}_2$ norm, that is,

$$\int_0^\infty \boldsymbol{u}^T\boldsymbol{u}\,\mathrm{d}t < \infty, \qquad \int_0^\infty \boldsymbol{v}^T\boldsymbol{v}\,\mathrm{d}t < \infty \tag{3}$$

Though the interceptor guidance problem has finite-time characteristics, there are precedences where the guidance laws have been derived from the infinite-horizon formulations of the optimal control/guidance problems and successfully applied [23,40,42]. For the present nonlinear differential game problem, which shares a close relation to nonlinear H_∞ problem [43], the formulation over infinite horizon can be justified in line with [44]. For a regulation problem, the disturbance $\boldsymbol{v}$ is said to be locally attenuated by a factor γ if the $\mathcal{L}_2$ norm of $\mathbf{y} = [\Xi(\boldsymbol{x})\boldsymbol{x}\ \boldsymbol{u}]$, where $\Xi(\boldsymbol{x})^T\Xi(\boldsymbol{x}) = \mathbf{Q}(\boldsymbol{x})$, satisfies the following relation:

$$\int_{t_0}^{t_f} \mathbf{y}^T\mathbf{y}\,\mathrm{d}t = \int_{t_0}^{t_f} (\boldsymbol{x}^T\mathbf{Q}(\boldsymbol{x})\boldsymbol{x} + \boldsymbol{u}^T\boldsymbol{u})\,\mathrm{d}t \le \gamma^2 \int_{t_0}^{t_f} \boldsymbol{v}^T\boldsymbol{v}\,\mathrm{d}t \tag{4}$$

for all $t_0 < t_f < \infty$ and for all $\boldsymbol{v} \in \mathcal{L}_2(t_0, t_f)$. This condition in Eq. (4) is satisfied if there exists an internal stabilizing controller such that the following condition is satisfied:

$$\int_{t_0}^{\infty} (\boldsymbol{x}^T\mathbf{Q}(\boldsymbol{x})\boldsymbol{x} + \boldsymbol{u}^T\boldsymbol{u})\,\mathrm{d}t \le \gamma^2 \int_{t_0}^{\infty} \boldsymbol{v}^T\boldsymbol{v}\,\mathrm{d}t \tag{5}$$

If there exists a solution of the max-min differential game problem,

$$\max_{\boldsymbol{v}\in L_2} \min_{\boldsymbol{u}\in L_2} \int_{t_0}^{\infty} (\boldsymbol{x}^T\mathbf{Q}(\boldsymbol{x})\boldsymbol{x} + \boldsymbol{u}^T\boldsymbol{u} - \boldsymbol{v}^T\boldsymbol{v})\,\mathrm{d}t \tag{6}$$

subject to the constraints in Eq. (2), then it satisfies the condition in Eq. (5) as well as the condition in Eq. (4).

If $\mathbf{f}(\boldsymbol{x}) \in \mathcal{C}^1$ such that $\mathbf{f}(\mathbf{0}) = \mathbf{0}$, then $\mathbf{f}(\boldsymbol{x})$ can be factorized (nonuniquely for $n > 1$) as $\mathbf{f}(\boldsymbol{x}) = \mathbf{A}(\boldsymbol{x})\boldsymbol{x}$. Then, Eq. (2) can be expressed in the following state-dependent coefficient (SDC) form:

$$\dot{\boldsymbol{x}} = \mathbf{A}(\boldsymbol{x})\boldsymbol{x} + \mathbf{B}(\boldsymbol{x})\boldsymbol{u} + \mathbf{C}(\boldsymbol{x})\boldsymbol{v}, \qquad \boldsymbol{x}(t_0) = \boldsymbol{x}_0 \tag{7}$$

In order that an SDC form be an admissible one, the criteria of pointwise controllability and pointwise observability need to be satisfied. Definitions of pointwise stabilizability, pointwise controllability, pointwise detectability, pointwise observability, and pointwise Hurwitz will be used subsequently in line with [37]. Note that the SDC form given in Eq. (7) is similar to the extended linearization technique given in [45] and used in [17].

Because the problem is formulated as zero-sum differential games, the concept of saddle-point equilibrium is pertinent here and is stated next.

Definition 1: The strategies $\boldsymbol{u}^*$ of $\mathcal{P}$ and $\boldsymbol{v}^*$ of $\mathcal{E}$ are saddle-point strategies of the game if, for any other strategy $\boldsymbol{u}$ used by $\mathcal{P}$ or any other strategy $\boldsymbol{v}$ used by $\mathcal{E}$, the following relation holds:

$$J(\boldsymbol{u}^*, \boldsymbol{v}) \le J(\boldsymbol{u}^*, \boldsymbol{v}^*) \le J(\boldsymbol{u}, \boldsymbol{v}^*) \tag{8}$$

A player cannot get optimum benefit from a game if it deviates from its optimal strategy while its opponent sticks to its optimal strategy. Thus, each player should look to play his/her own optimal strategy. If there exists a continuously differentiable, positive-valued, stabilizing solution $\mathcal{W}$: $\mathbb{R}^n \to \mathbb{R}$ to the HJBI equation

$$\nabla\mathcal{W}^T\mathbf{f}(\boldsymbol{x}) - \frac{1}{2}\nabla\mathcal{W}^T(\mathbf{B}(\boldsymbol{x})\mathbf{B}^T(\boldsymbol{x}) - \gamma^{-2}\mathbf{C}(\boldsymbol{x})\mathbf{C}^T(\boldsymbol{x}))\nabla\mathcal{W} + \frac{1}{2}\boldsymbol{x}^T\mathbf{Q}(\boldsymbol{x})\boldsymbol{x} = 0, \qquad \mathcal{W}(\mathbf{0}) = 0 \tag{9}$$

where $\nabla\mathcal{W} = \partial\mathcal{W}/\partial\boldsymbol{x}$, then the saddle-point strategies are obtained to be $\boldsymbol{u}^* = -\mathbf{B}^T(\boldsymbol{x})\nabla\mathcal{W}(\boldsymbol{x})\boldsymbol{x}$ and $\boldsymbol{v}^* = \gamma^{-2}\mathbf{C}^T(\boldsymbol{x})\nabla\mathcal{W}(\boldsymbol{x})\boldsymbol{x}$ [35]. It is assumed here that $\mathbf{R}_1 = \mathbf{I}_{n_p}$ and $\mathbf{R}_2 = \mathbf{I}_{n_e}$.

As it is already discussed in Sec. I, obtaining an analytic closed-form solution to the associated HJBI partial differential equation in Eq. (9) is almost impossible when the state equations are nonlinear. In the following, the SDRE method is presented for zero-sum differential games. Then, the aspects of optimality and stability of the proposed solution are discussed.

If there exists a unique, symmetric, positive-definite solution $\mathbf{P}(\boldsymbol{x}) \in \mathbb{R}^{n\times n}$ to the following matrix SDRE:

$$\mathbf{A}^T(\boldsymbol{x})\mathbf{P}(\boldsymbol{x}) + \mathbf{P}(\boldsymbol{x})\mathbf{A}(\boldsymbol{x}) - \mathbf{P}(\boldsymbol{x})(\mathbf{B}(\boldsymbol{x})\mathbf{R}_1^{-1}(\boldsymbol{x})\mathbf{B}^T(\boldsymbol{x}) - \gamma^{-2}\mathbf{C}(\boldsymbol{x})\mathbf{R}_2^{-1}(\boldsymbol{x})\mathbf{C}^T(\boldsymbol{x}))\mathbf{P}(\boldsymbol{x}) + \mathbf{Q}(\boldsymbol{x}) = \mathbf{0} \tag{10}$$

then the strategy for $\mathcal{P}$ corresponding to the state $\boldsymbol{x}$. is proposed as

$$\boldsymbol{u}_\bullet = -\mathbf{R}_1^{-1}(\boldsymbol{x})\mathbf{B}^T(\boldsymbol{x})\mathbf{P}(\boldsymbol{x})\boldsymbol{x} \tag{11}$$

Theorem 1: In the general multivariable case, the proposed SDRE nonlinear feedback stratgey for $\mathcal{P}$, given in Eq. (11), satisfies the following the first-order necessary condition:

$$\boldsymbol{u}_\bullet = \arg\min_{\boldsymbol{u}} H \tag{12}$$

where $\mathcal{H}$ is the Hamiltonian of the system.

Proof: The Hamiltonian associated with the nonlinear min-max problem is given by

$$\mathcal{H} = \frac{1}{2}\boldsymbol{x}^T\mathbf{Q}(\boldsymbol{x})\boldsymbol{x} + \frac{1}{2}\boldsymbol{u}^T\mathbf{R}_1(\boldsymbol{x})\boldsymbol{u} - \frac{\gamma^2}{2}\boldsymbol{v}^T\mathbf{R}_2(\boldsymbol{x})\boldsymbol{v} + \boldsymbol{\lambda}^T(\mathbf{A}(\boldsymbol{x})\boldsymbol{x} + \mathbf{B}(\boldsymbol{x})\boldsymbol{u} + \mathbf{C}(\boldsymbol{x})\boldsymbol{v}) \tag{13}$$

where $\boldsymbol{\lambda} \in \mathbb{R}^n$ is the costate vector. For the nonlinear min-max problem, let it be assumed that the costate vector $\boldsymbol{\lambda}$ is associated with the state vector $\boldsymbol{x}$ by the following relation:

$$\boldsymbol{\lambda} = \mathbf{P}(\boldsymbol{x})\boldsymbol{x} \tag{14}$$

To minimize $\mathcal{H}$, $\mathcal{P}$'s control $\boldsymbol{u}$ has to satisfy

$$\partial\mathcal{H}/\partial\boldsymbol{u} = \mathbf{0} \Rightarrow \boldsymbol{u} = -\mathbf{R}_1^{-1}(\boldsymbol{x})\mathbf{B}^T(\boldsymbol{x})\boldsymbol{\lambda} \tag{15}$$

Substituting Eq. (14) in Eq. (15) yields the control in Eq. (11).

Remark 1: Similarly, $\mathcal{E}$'s strategy to maximize $\mathcal{H}$ is obtained as

$$\boldsymbol{v}_{\text{worst}} = \gamma^{-2}\mathbf{R}_2^{-1}(\boldsymbol{x})\mathbf{C}^T(\boldsymbol{x})\mathbf{P}(\boldsymbol{x})\boldsymbol{x} \tag{16}$$

Theorem 2: Assume that the functions $\mathbf{A}(\boldsymbol{x})$, $\mathbf{B}(\boldsymbol{x})$, $\mathbf{C}(\boldsymbol{x})$, $\mathbf{P}(\boldsymbol{x})$, $\mathbf{Q}(\boldsymbol{x})$, $\mathbf{R}_1(\boldsymbol{x})$, $\mathbf{R}_2(\boldsymbol{x})$, along with their gradients $\mathbf{A}_{x_i}(\boldsymbol{x})$, $\mathbf{B}_{x_i}(\boldsymbol{x})$, $\mathbf{C}_{x_i}(\boldsymbol{x})$, $\mathbf{P}_{x_i}(\boldsymbol{x})$, $\mathbf{Q}_{x_i}(\boldsymbol{x})$, $\mathbf{R}_{1x_i}(\boldsymbol{x})$, $\mathbf{R}_{2x_i}(\boldsymbol{x})$, $i = 1, 2, \ldots n$, are

bounded in the neighborhood Ω about the origin. Then, in the general multivariable case, under asymptotic stability, as the state $\boldsymbol{x}$ is driven to $\mathbf{0}$, the SDRE nonlinear feedback solution and its associated state and costate trajectories asymptotically approach to satisfy the equation $\dot{\boldsymbol{\lambda}} = -\partial H/\partial \boldsymbol{x}$ at a quadratic rate.

Proof: If Isaacs's condition is satisfied [46], then $\mathcal{P}$'s strategy $\boldsymbol{u}_\bullet$ in Eq. (15) and $\mathcal{E}$'s strategy $\boldsymbol{v}_{\text{worst}}$ in Eq. (16) constitute saddle-point strategies if the associated state $\boldsymbol{x}$ and costate $\boldsymbol{\lambda}$ trajectories satisfy the second necessary condition:

$$\begin{aligned}\dot{\boldsymbol{\lambda}} &= -\partial \mathcal{H}(\boldsymbol{u}, \boldsymbol{v})/\partial \boldsymbol{x} \\ &= -\frac{\partial \mathbf{f}^T}{\partial \boldsymbol{x}}\boldsymbol{\lambda} - \boldsymbol{u}^T\frac{\partial \mathbf{B}^T}{\partial \boldsymbol{x}}\boldsymbol{\lambda} - \boldsymbol{v}^T\frac{\partial \mathbf{C}^T}{\partial \boldsymbol{x}}\boldsymbol{\lambda} - \mathbf{Q}\boldsymbol{x} - \frac{1}{2}\boldsymbol{x}^T\frac{\partial \mathbf{Q}(\boldsymbol{x})}{\partial \boldsymbol{x}}\boldsymbol{x} \\ &\quad -\frac{1}{2}\boldsymbol{u}^T\frac{\partial \mathbf{R}_1(\boldsymbol{x})}{\partial \boldsymbol{x}}\boldsymbol{u} + \frac{\gamma^2}{2}\boldsymbol{v}^T\frac{\partial \mathbf{R}_2(\boldsymbol{x})}{\partial \boldsymbol{x}}\boldsymbol{v} \end{aligned} \tag{17}$$

For details of the derivation of the condition in Eq. (17), refer to [47]. Differentiating Eq. (14) with respect to time yields

$$\dot{\boldsymbol{\lambda}} = \dot{\mathbf{P}}(\boldsymbol{x})\boldsymbol{x} + \mathbf{P}(\boldsymbol{x})\dot{\boldsymbol{x}} \tag{18}$$

When $\boldsymbol{u} = \boldsymbol{u}_\bullet = -\mathbf{R}_1^{-1}(\boldsymbol{x})\mathbf{B}^T(\boldsymbol{x})\mathbf{P}(\boldsymbol{x})\boldsymbol{x}$ and $\boldsymbol{v} = \boldsymbol{v}_{\text{worst}} = \gamma^{-2}\mathbf{R}_2^{-1}(\boldsymbol{x})\mathbf{C}^T(\boldsymbol{x})\mathbf{P}(\boldsymbol{x})\boldsymbol{x}$, then using Eqs. (7), (17), and (18), the following expression is obtained for $\dot{\mathbf{P}}\boldsymbol{x}$:

$$\begin{aligned}\dot{\mathbf{P}}\boldsymbol{x} &= \boldsymbol{x}^T\mathbf{P}\mathbf{B}\mathbf{R}_1^{-1}\frac{\partial \mathbf{B}^T}{\partial \boldsymbol{x}}\mathbf{P}\boldsymbol{x} - \boldsymbol{x}^T\mathbf{P}\mathbf{C}\mathbf{R}_2^{-1}\frac{\partial \mathbf{C}^T}{\partial \boldsymbol{x}}\mathbf{P}\boldsymbol{x} - \frac{1}{2}\boldsymbol{x}^T\frac{\partial \mathbf{Q}}{\partial \boldsymbol{x}}\boldsymbol{x} \\ &\quad -\frac{1}{2}\boldsymbol{x}^T\mathbf{P}\mathbf{B}\mathbf{R}_1^{-1}\frac{\partial \mathbf{R}_1}{\partial \boldsymbol{x}}\mathbf{R}_1^{-1}\mathbf{B}^T\mathbf{P}\boldsymbol{x} \\ &\quad +\frac{\gamma^{-2}}{2}\boldsymbol{x}^T\mathbf{P}\mathbf{C}\mathbf{R}_2^{-1}\frac{\partial \mathbf{R}_2}{\partial \boldsymbol{x}}\mathbf{R}_2^{-1}\mathbf{C}^T\mathbf{P}\boldsymbol{x} \\ &\quad -(\mathbf{A}^T\mathbf{P} + \mathbf{P}\mathbf{A} - \mathbf{P}\mathbf{B}\mathbf{R}_1^{-1}\mathbf{B}^T\mathbf{P} + \gamma^{-2}\mathbf{C}\mathbf{R}_2^{-1}\mathbf{C}^T\mathbf{P} + \mathbf{Q})\boldsymbol{x} \end{aligned} \tag{19}$$

where $\partial \mathbf{Q}/\partial \boldsymbol{x}$, $\partial \mathbf{R}_1/\partial \boldsymbol{x}$, $\partial \mathbf{R}_2/\partial \boldsymbol{x}$, $\partial \mathbf{A}^T/\partial \boldsymbol{x}$, $\partial \mathbf{B}^T/\partial \boldsymbol{x}$, $\partial \mathbf{C}^T/\partial \boldsymbol{x}$ generate tensors. The argument $\boldsymbol{x}$ is dropped for brevity. Imposing Eq. (10) in Eq. (19) yields

$$\begin{aligned}\dot{\mathbf{P}}\boldsymbol{x} &= \boldsymbol{x}^T\mathbf{P}\mathbf{B}\mathbf{R}_1^{-1}\frac{\partial \mathbf{B}^T}{\partial \boldsymbol{x}}\mathbf{P}\boldsymbol{x} - \boldsymbol{x}^T\mathbf{P}\mathbf{C}\mathbf{R}_2^{-1}\frac{\partial \mathbf{C}^T}{\partial \boldsymbol{x}}\mathbf{P}\boldsymbol{x} - \frac{1}{2}\boldsymbol{x}^T\frac{\partial \mathbf{Q}}{\partial \boldsymbol{x}}\boldsymbol{x} \\ &\quad -\frac{1}{2}\boldsymbol{x}^T\mathbf{P}\mathbf{B}\mathbf{R}_1^{-1}\frac{\partial \mathbf{R}_1}{\partial \boldsymbol{x}}\mathbf{R}_1^{-1}\mathbf{B}^T\mathbf{P}\boldsymbol{x} \\ &\quad +\frac{\gamma^{-2}}{2}\boldsymbol{x}^T\mathbf{P}\mathbf{C}\mathbf{R}_2^{-1}\frac{\partial \mathbf{R}_2}{\partial \boldsymbol{x}}\mathbf{R}_2^{-1}\mathbf{C}^T\mathbf{P}\boldsymbol{x} \end{aligned} \tag{20}$$

Whenever the condition in Eq. (20) holds, the closed-loop solution satisfies all the first-order necessary conditions. Even when the state equations in Eq. (2) and objective function (1) together satisfy Isaacs's condition, the necessary condition in Eq. (20) for game theoretic saddle point may not be satisfied for a given SDC parameterization in the multivariable case. Under asymptotic stability, as $\boldsymbol{x}$ is driven to zero, the second necessary condition for saddle point ($\dot{\boldsymbol{\lambda}} = -[\partial H(\boldsymbol{u}, \boldsymbol{v})/\partial \boldsymbol{x}]$) is asymptotically satisfied at a quadratic rate. The rest of the proof is in line with the one in [37]. □

Theorem 3: Assume that the SDC parameterization is chosen such that $\mathbf{A}(\cdot) \in \mathcal{C}^1$ in the neighborhood Ω about the origin and that the pairs $\{\mathbf{A}(\boldsymbol{x}), \mathbf{B}(\boldsymbol{x})\}$, $\{\mathbf{A}(\boldsymbol{x}), \mathbf{C}(\boldsymbol{x})\}$ are pointwise controllable, and $\{\mathbf{Q}^{1/2}(\boldsymbol{x}), \mathbf{A}(\boldsymbol{x})\}$ is pointwise observable $\forall\ \boldsymbol{x} \in \Omega$. For a given γ, if $\forall\ \boldsymbol{x} \in \Omega$, a unique, symmetric, positive-definite solution $\mathbf{P}(\boldsymbol{x})$ exists to the SDRE in Eq. (10) corresponding to the state $\boldsymbol{x}$, then the proposed SDRE nonlinear feedback control in Eq. (11) produces a closed-loop solution that is locally asymptotically stable when $(a)\boldsymbol{v} = \mathbf{0}$ and $(b)\boldsymbol{v} = \boldsymbol{v}_{\text{worst}} = \gamma^{-2}\mathbf{C}^T(\boldsymbol{x})\mathbf{P}(\boldsymbol{x})\boldsymbol{x}$.

Proof: Without any loss of generality, it is assumed here that $\mathbf{R}_1(\boldsymbol{x}) = \mathbf{I}_{n_p}$ and $\mathbf{R}_2(\boldsymbol{x}) = \mathbf{I}_{n_e}$ for all $\boldsymbol{x}$.

Corresponding to the state vector $\boldsymbol{x} \in \mathbb{R}^n$, the unique, symmetric, positive-definite solution to the SDRE in Eq. (10) is $\mathbf{P}(\boldsymbol{x})$. With $\boldsymbol{u} = -\mathbf{B}^T(\boldsymbol{x})\mathbf{P}(\boldsymbol{x})\boldsymbol{x}$, the state equations take the following closed-loop forms:

$$\dot{\boldsymbol{x}} = \mathbf{A}(\boldsymbol{x}) - \mathbf{B}(\boldsymbol{x})\mathbf{B}^T(\boldsymbol{x})\mathbf{P}(\boldsymbol{x}) = \mathbf{A}_{CL}(\boldsymbol{x})\boldsymbol{x} \tag{21}$$

$$\dot{\boldsymbol{x}} = \mathbf{A}(\boldsymbol{x}) - \mathbf{B}(\boldsymbol{x})\mathbf{B}^T(\boldsymbol{x})\mathbf{P}(\boldsymbol{x}) + \gamma^{-2}\mathbf{C}(\boldsymbol{x})\mathbf{C}^T(\boldsymbol{x})\mathbf{P}(\boldsymbol{x}) = \mathbf{A}_{CL_v}(\boldsymbol{x})\boldsymbol{x} \tag{22}$$

when $\boldsymbol{v} = \mathbf{0}$ and $\boldsymbol{v} = \gamma^{-2}\mathbf{C}^T(\boldsymbol{x})\mathbf{P}(\boldsymbol{x})\boldsymbol{x}$, respectively.

In [48] (Theorem 4.8), it was proved that, under the assumptions that the pairs $\{\hat{\mathbf{A}}, \hat{\mathbf{B}}\}$ and $\{\hat{\mathbf{A}}, \hat{\mathbf{C}}\}$ are controllable and $\{\hat{\mathbf{Q}}^{1/2}, \hat{\mathbf{A}}\}$ is observable, if the following algebraic Riccati equation:

$$\hat{\mathbf{A}}^T\Pi + \Pi\hat{\mathbf{A}} - \Pi(\hat{\mathbf{B}}\hat{\mathbf{B}}^T - \gamma^{-2}\hat{\mathbf{C}}\hat{\mathbf{C}}^T)\Pi + \hat{Q} = \mathbf{0} \tag{23}$$

admits a minimal positive-definite solution $\Pi^+(\gamma)$ for a given γ, then the two feedback matrices $\mathbf{A}_F = \hat{\mathbf{A}} - \hat{\mathbf{B}}\hat{\mathbf{B}}^T\Pi^+$ and $\mathbf{A}_{F_v} = \hat{\mathbf{A}} - (\hat{\mathbf{B}}\hat{\mathbf{B}}^T\Pi^+ - \gamma^{-2}\hat{\mathbf{C}}\hat{\mathbf{C}}^T\Pi^+)$ are Hurwitz.

From this argument, it can be shown that the two feedback matrices $\mathbf{A}_{CL}(\boldsymbol{x})$ and $\mathbf{A}_{CL_v}(\boldsymbol{x})$ are Hurwitz in a pointwise sense because, from the assumptions that $\mathbf{A}(\cdot)$, $\mathbf{B}(\cdot)$, $\mathbf{C}(\cdot) \in \mathcal{C}^1(\mathbb{R}^n)$, it follows that $\mathbf{P}(\boldsymbol{x}) \in \mathcal{C}^1(\mathbb{R}^n)$. Moreover, it also follows that $\mathbf{A}_{CL}(\boldsymbol{x}) \in \mathcal{C}^1(\mathbb{R}^n)$ and $\mathbf{A}_{CL_v}(\boldsymbol{x}) \in \mathcal{C}^1(\mathbb{R}^n)$. Applying the mean-value theorem to $\mathbf{A}_{CL}(\boldsymbol{x})$ gives

$$\mathbf{A}_{CL}(\boldsymbol{x}) = \mathbf{A}_{CL}(\mathbf{0}) + (\partial \mathbf{A}_{CL}(\zeta)/\partial \boldsymbol{x})\boldsymbol{x} \tag{24}$$

where ζ is a point on the line segment joining the origin $\mathbf{0}$ and $\boldsymbol{x}$ satisfying the previous equation, and $(\partial \mathbf{A}_{CL}(\zeta)/\partial \boldsymbol{x})$ is a tensor. Substituting $\mathbf{A}_{CL}(\boldsymbol{x})$ from Eq. (24) into Eq. (21), the following closed-loop dynamics is obtained:

$$\dot{\boldsymbol{x}} = \mathbf{A}_{CL}(\mathbf{0})\boldsymbol{x} + \Psi(\boldsymbol{x}, \zeta)\|\boldsymbol{x}\| \tag{25}$$

where $\Psi(\boldsymbol{x}, \zeta) = (1/\|\boldsymbol{x}\|)\boldsymbol{x}^T(\partial \mathbf{A}_{CL}(\zeta)/\partial \boldsymbol{x})\boldsymbol{x}$, such that $\lim_{\|\boldsymbol{x}\|\to 0}\Psi(\boldsymbol{x}, \zeta) = \mathbf{0}$.

In a neighborhood about the origin, local asymptotic stability is obtained where the linear term having a constant stable coefficient matrix $\mathbf{A}_{CL}(\mathbf{0})$ dominates the higher-order term.

Under the same assumptions, local asymptotic stability can be proved in a similar way when $\boldsymbol{v} = \gamma^{-2}\mathbf{C}^T(\boldsymbol{x})\mathbf{P}(\boldsymbol{x})\boldsymbol{x}$. □

Though conditions that ensure local asymptotic stability in a neighborhood around the origin have been derived previously, it is expedient to investigate if an equilibrium is globally asymptotically stable. In the next theorem, the conditions for global asymptotic stability are stated. The argument $\boldsymbol{x}$ is dropped for brevity.

Theorem 4: When an SDC parameterization is controllable and observable, then the control given in Eq. (15) makes the equilibrium at the origin globally asymptotically stable when $\boldsymbol{v} = \mathbf{0}$ if $\dot{\mathbf{P}} < \mathbf{Q}$ and $\mathbf{Q} > \mathbf{0}$ for all $\boldsymbol{x}$.

Proof: This can be proved in the same line with [49]. □

III. Application to Impact-Angle-Constrained Guidance Problem

In the engagement geometry shown in Fig. 1, V_I and V_T are the velocity vectors, α and β are the flight-path angles (FPA), and u and v are the control vectors perpendicular to the velocity vectors of the interceptor and the target, respectively. The interceptor and the target are assumed to have constant speeds. The line-of-sight (LOS) angle is given by θ. The LOS rate $\dot{\theta}$ is designated by σ. The distance of the target from the interceptor along the LOS is r. The interceptor is required to intercept the target at an angle η^C. The kinematics of the interceptor–target engagement system are given by the following equations:

$$\dot{r} = V_r = -V_T\cos(\beta + \theta) - V_I\cos(\alpha - \theta) \tag{26}$$

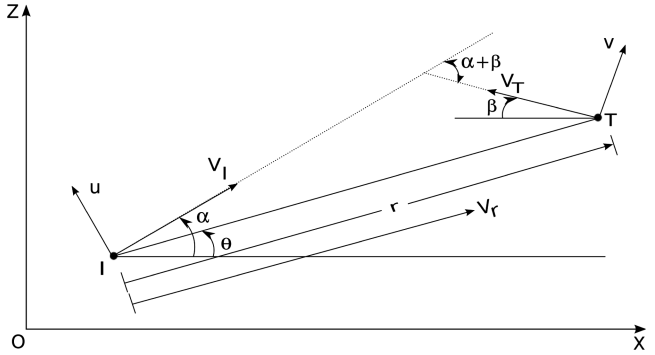

Fig. 1 Engagement geometry with given intercept angle.

$$\dot{\theta} = \sigma = (V_T \sin(\beta + \theta) - V_I \sin(\alpha - \theta))/r \tag{27}$$

$$\dot{\alpha} = u/V_I \tag{28}$$

$$\dot{\beta} = v/V_T \tag{29}$$

A. Guidance Principle

To ensure capture, the interceptor has to impose a hard constraint of zero terminal miss distance and zero error on the terminal impact angle. But a smart target will try to maximize the terminal distance as well as the terminal impact-angle error in this case. Thus, the problem is posed in a form where the interceptor tries to minimize terminal miss distance along with terminal impact-angle error, whereas the target tries to maximize these quantities. In this regard, two terms are introduced in the following.

Definition 2 (zero-effort miss): The quantity zero-effort miss, designated by r_{miss}, at an instant t is defined as the closest distance between the interceptor and the target if, from the instant t onward, both the interceptor and the target do not maneuver. The expression for $r_{\text{miss}}(t)$ comes out to be

$$r_{\text{miss}}(t) = \frac{r^2\sigma}{\sqrt{\dot{r}^2 + r^2\sigma^2}} \tag{30}$$

The derivation of the expression for r_{miss} in Eq. (30) is standard and can be found in [50].

Another quantity related to impact-angle-constrained guidance is defined here in line with [17].

Definition 3 (projected terminal impact angle): The projected terminal impact angle (PTIA) at an instant t is defined as the angle between the velocity vectors of the interceptor and the target at the instant of their closest proximity, if both the interceptor and the target do not execute any further maneuvers from the time instant t onward:

$$\eta = (\alpha - \theta) + (\beta + \theta) = \alpha + \beta \tag{31}$$

The error between PTIA η and the desired impact angle η^C is

$$\xi = \eta - \eta^C = \alpha + \beta - \eta^C \tag{32}$$

From the expression of r_{miss} in Eq. (30), it can be seen that regulating σ to zero implies regulation of r_{miss} to zero value. Regulation of σ to zero while keeping $V_r < 0$ leads to interception. In addition, ξ needs to be regulated to zero to achieve interception at the desired impact angle. Based on the factor that the interceptor needs to regulate σ and ξ to zero values to intercept the target at a desired impact angle, the states are chosen as

$$\boldsymbol{x} = [\sigma \quad \xi]^T \tag{33}$$

The dynamics for the state σ is obtained as follows:

$$\begin{aligned}
\frac{\mathrm{d}}{\mathrm{d}t}(r\sigma) = \frac{\mathrm{d}}{\mathrm{d}t}(r\dot{\theta}) &= \frac{\mathrm{d}}{\mathrm{d}t}[V_T \sin(\beta + \theta) - V_I \sin(\alpha - \theta)] \\
\dot{r}\sigma + r\dot{\sigma} = \dot{r}\dot{\theta} + r\ddot{\theta} &= (V_T \cos(\beta + \theta) + V_I \cos(\alpha - \theta))\dot{\theta} \\
&\quad - \dot{\alpha}V_I \cos(\alpha - \theta) + \dot{\beta}V_T \cos(\beta + \theta) \\
\dot{\sigma} = \ddot{\theta} &= -2\dot{r}\dot{\theta}/r - u \cos(\alpha - \theta)/r + v \cos(\beta + \theta)/r
\end{aligned} \tag{34}$$

The dynamics of the state ξ is obtained as follows:

$$\xi = \alpha + \beta - \eta^C \quad \dot{\xi} = \dot{\alpha} + \dot{\beta} \quad = u/V_I + v/V_T \tag{35}$$

Thus, the dynamic equations of the states take the following form:

$$\dot{\sigma} = 2(-V_r/r)\sigma - u \cos(\alpha - \theta)/r + v \cos(\beta + \theta)/r \tag{36a}$$

$$\dot{\xi} = u/V_I + v/V_T \tag{36b}$$

Note that, in this problem, $\boldsymbol{u} = u$ and $\boldsymbol{v} = v$.

B. State-Dependent Coefficient Form of State Equations

The state equations given in Eq. (36) can be expressed in the SDC form like Eq. (7), where

$$\mathbf{A}(\boldsymbol{x}) = \begin{bmatrix} -2V_r/r & 0 \\ 0 & 0 \end{bmatrix} \tag{37}$$

$$\mathbf{B}(\boldsymbol{x}) = \begin{bmatrix} -\cos(\alpha - \theta)/r \\ 1/V_I \end{bmatrix} \tag{38}$$

$$\mathbf{C}(\boldsymbol{x}) = \begin{bmatrix} \cos(\beta + \theta)/r \\ 1/V_T \end{bmatrix} \tag{39}$$

Note that the matrices $\mathbf{B}(\boldsymbol{x})$ and $\mathbf{C}(\boldsymbol{x})$ are not dependent on time-to-go, unlike the formulation in [17].

The following notations will be used for the elements of $\mathbf{A}$, $\mathbf{B}$, and $\mathbf{C}$ to facilitate subsequent analysis:

$$a = \mathbf{A}(1,1) = -2V_r/r \tag{40}$$

$$b_1 = \mathbf{B}(1,1) = -\cos(\alpha - \theta)/r, \qquad b_2 = \mathbf{B}(2,1) = 1/V_I \tag{41}$$

$$c_1 = \mathbf{C}(1,1) = \cos(\beta + \theta)/r, \qquad c_2 = \mathbf{C}(2,1) = 1/V_T \tag{42}$$

The terms $(\alpha - \theta)$ and $(\beta + \theta)$, which occur in the elements of the SDC matrices $\mathbf{A}(\boldsymbol{x})$, $\mathbf{B}(\boldsymbol{x})$, and $\mathbf{C}(\boldsymbol{x})$, have the following expressions in terms of the states σ and ξ:

$$\alpha - \theta = \tan^{-1}\left(\frac{V_T \sin(\xi + \eta^c)}{V_T \cos(\xi + \eta^c) + V_M}\right) - \sin^{-1}\left(\frac{r\sigma}{\vartheta}\right) \tag{43}$$

$$\beta + \theta = \tan^{-1}\left(\frac{V_M \sin(\xi + \eta^c)}{V_M \cos(\xi + \eta^c) + V_T}\right) + \sin^{-1}\left(\frac{r\sigma}{\vartheta}\right) \tag{44}$$

where $\vartheta = \sqrt{V_T^2 + V_M^2 + 2V_M V_T \cos(\xi + \eta^c)}$. The full SDC form is obtained by substituting the expressions of $(\alpha - \theta)$ and $(\beta + \theta)$

from Eqs. (44) and (45), respectively, where they occur in the elements of the SDC matrices.

In order that the SDC form be an admissible one, the pairs $\{\mathbf{A}(\boldsymbol{x}), \mathbf{B}(\boldsymbol{x})\}$ and $\{\mathbf{A}(\boldsymbol{x}), \mathbf{C}(\boldsymbol{x})\}$ should be pointwise controllable. The following matrices:

$$[\,\mathbf{B}(\boldsymbol{x}) \quad \mathbf{A}(\boldsymbol{x})\mathbf{B}(\boldsymbol{x})\,] = \begin{bmatrix} b_1 & ab_1 \\ b_2 & 0 \end{bmatrix} \tag{45}$$

and

$$[\,\mathbf{C}(\boldsymbol{x}) \quad \mathbf{A}(\boldsymbol{x})\mathbf{C}(\boldsymbol{x})\,] = \begin{bmatrix} c_1 & ac_1 \\ c_2 & 0 \end{bmatrix} \tag{46}$$

have rank 2 as long as $ab_1 \neq 0$ and $ac_1 \neq 0$, respectively. This implies that pointwise controllability condition is satisfied for $(\alpha - \theta) \neq \pi/2$ and $(\beta + \theta) \neq \pi/2$, respectively, as long as $V_r \neq 0$ and $r \neq 0$.

The other condition of an SDC form to be admissible is that the pair $\{\mathbf{Q}^{1/2}(\boldsymbol{x}), \mathbf{A}(\boldsymbol{x})\}$ has to be pointwise observable. The 2×2 state weighing matrix $\mathbf{Q}(\boldsymbol{x})$ is chosen to be of the following form:

$$\mathbf{Q}(\boldsymbol{x}) = \begin{bmatrix} q_\sigma(\boldsymbol{x}) & 0 \\ 0 & q_\xi(\boldsymbol{x}) \end{bmatrix} \tag{47}$$

where $q_\sigma(\boldsymbol{x})$ and $q_\xi(\boldsymbol{x})$ are the weights on the states σ and ξ, respectively. With the choice of the weights $q_\sigma(\boldsymbol{x}) > 0$, and $q_\xi(\boldsymbol{x}) > 0$ for all $\boldsymbol{x}$, the following matrix:

$$\begin{bmatrix} \mathbf{Q}^{1/2}(\boldsymbol{x}) \\ \mathbf{Q}^{1/2}(\boldsymbol{x})\mathbf{A}(\boldsymbol{x}) \end{bmatrix} = \begin{bmatrix} \sqrt{q_\sigma} & 0 \\ 0 & \sqrt{q_\xi} \\ \sqrt{q_\sigma}a & 0 \\ 0 & 0 \end{bmatrix} \tag{48}$$

has rank 2, that is, the pointwise observability criterion is satisfied as long as $V_r \neq 0$ and $r \neq 0$.

The domain over which the given SDC form remains admissible is

$$D_{\mathrm{SDC}} = \{\boldsymbol{x}\colon V_r \neq 0, r \neq 0, |(\alpha - \theta)| \neq \pi/2, |(\beta + \theta)| \neq \pi/2\} \tag{49}$$

The elements of the symmetric matrix $\mathbf{F}$ are

$$\mathbf{F}(1,1) = f_1 = b_1^2 - c_1^2/\gamma^2 \tag{51a}$$

$$\mathbf{F}(1,2) = \mathbf{F}(2,1) = f_2 = b_1 b_2 - c_1 c_2/\gamma^2 \tag{51b}$$

$$\mathbf{F}(2,2) = f_3 = b_2^2 - c_2^2/\gamma^2 \tag{51c}$$

The eigenvalues of $\mathbf{H}$ are

$$\mathrm{eig}(\mathbf{H}) = \left\{\sqrt{\delta + \Delta}, \sqrt{\delta - \Delta}, -\sqrt{\delta + \Delta}, -\sqrt{\delta - \Delta}\right\} \tag{52}$$

where

$$\delta = a^2 + f_1 q_\sigma + f_3 q_\xi \tag{53}$$

$$\Delta = \sqrt{a^4 + 2a^2 f_1 q_\sigma - 2a^2 f_3 q_\xi + f_1^2 q_\sigma^2 - 2f_1 f_3 q_\sigma q_\xi + 4f_2^2 q_\sigma q_\xi + f_3^2 q_\xi^2} \tag{54}$$

where a is given by Eq. (40); b_1, b_2 are given by Eq. (41); and c_1, c_2 are given by Eq. (42).

The existence of the solution of the algbraic Riccati equation in Eq. (10) imposes the condition that there should be no eigenvalue of $\mathbf{H}$ on the imaginary axis [51]. The eigenvalues of the Hamiltonian matrix $\mathbf{H}$ in Eq. (51) do not lie on the imaginary axis if

$$\Delta > 0, \qquad \delta > \Delta \tag{55}$$

The weights q_σ and q_ξ have to be positive and should be selected to satisfy Eq. (55) for all $\boldsymbol{x}$. If the poles of $\mathbf{H}$ are too close to the imaginary axis, then the Schur method, which is employed to compute the solution to the SDRE, fails.

The solution to the SDRE, $\mathbf{P}(\boldsymbol{x})$, is computed using Schur's algorithm [51,52]. The matrix composed of the eigenvectors corresponding to the negative eigenvalues $-\sqrt{\delta + \Delta}$ and $-\sqrt{\delta - \Delta}$ of $\mathbf{H}$ is

$$\mathbf{V} = \begin{bmatrix} \mathbf{V}_1 \\ \cdots \\ \mathbf{V}_2 \end{bmatrix} = \begin{bmatrix} ((\delta - 2f_3 q_\xi)/2 + \Delta/2)\left(\sqrt{\delta + \Delta} - a\right) & ((\delta - 2f_3 q_\xi)/2 - \Delta/2)\left(\sqrt{\delta - \Delta} - a\right) \\ \sqrt{\delta/2 + \Delta/2} & \sqrt{\delta/2 - \Delta/2} \\ ((\delta - 2f_3 q_\xi)/2 + \Delta/2) & ((\delta - 2f_3 q_\xi)/2 - \Delta/2) \\ 1 & 1 \end{bmatrix}$$

C. State-Dependent Riccati Equation Solution Method

The SDRE-based impact-angle-constrained guidance law depends on the solution of the SDRE given in Eq. (10), where $\mathbf{A}(\boldsymbol{x})$, $\mathbf{B}(\boldsymbol{x})$ and $\mathbf{C}(\boldsymbol{x})$ now have the expressions in Eqs. (37–39), respectively. Here, the conditions are investigated for existence of a positive-definite solution to the Riccati equation in Eq. (10).

It is assumed here that $\mathbf{R}_1(\boldsymbol{x}) = 1$ and $\mathbf{R}_2(\boldsymbol{x}) = 1$. The Hamiltonian matrix that is required to compute the solution of the Riccati equation in Eq. (10) corresponding to a state vector $\boldsymbol{x}$ is

$$\mathbf{H}(\boldsymbol{x}) = \begin{bmatrix} \mathbf{A}(\boldsymbol{x}) & -\mathbf{F}(\boldsymbol{x}) \\ -\mathbf{Q}(\boldsymbol{x}) & -\mathbf{A}^T(\boldsymbol{x}) \end{bmatrix} \tag{50}$$

where $\mathbf{F} = \mathbf{B}\mathbf{B}^T - \gamma^{-2}\mathbf{C}\mathbf{C}^T$.

The solution matrix $\mathbf{P}$ is computed from $\mathbf{V}_1$ and $\mathbf{V}_2$ as follows:

$$\mathbf{P} = \mathbf{V}_2\mathbf{V}_1^{-1} \quad = \begin{bmatrix} p_1/\Lambda & p_2/\Lambda \\ p_2/\Lambda & p_3/\Lambda \end{bmatrix} \tag{56}$$

where

$$p_1 = \sqrt{2}q_\sigma\Big((\delta - 2f_3 q_\xi - \Delta)\sqrt{\delta + \Delta} - (\delta - 2f_3 q_\xi + \Delta)\sqrt{\delta - \Delta}\Big) \tag{57a}$$

$$p_2 = 2\sqrt{2} f_2 q_\sigma q_\xi \left(\sqrt{\delta + \Delta} - \sqrt{\delta - \Delta} \right) \tag{57b}$$

$$p_3 = 4a q_\xi \Delta + \sqrt{2} q_\xi \Big((\delta - 2 f_3 q_\xi + \Delta)\sqrt{\delta - \Delta} - (\delta - 2 f_3 q_\xi - \Delta)\sqrt{\delta + \Delta} \Big) \tag{57c}$$

$$\Lambda = (\delta - \Delta)^{3/2}(\delta + \Delta)^{1/2} - (\delta - \Delta)^{1/2}(\delta + \Delta)^{3/2} + \sqrt{2} a (\delta - \Delta)^{1/2}(\delta - 2 f_3 q_\xi + \Delta) - \sqrt{2} a (\delta + \Delta)^{1/2}(\delta - 2 f_3 q_\xi - \Delta) \tag{57d}$$

For a given state vector $\boldsymbol{x}$ and a given value of γ, the matrix $\mathbf{P}(\boldsymbol{x})$ is positive-definite with proper selection of the state weights q_σ and q_ξ. For positive-definiteness of $\mathbf{P}(\boldsymbol{x})$, the following conditions should hold well:

$$(p_1 + p_3)/\Lambda > 0 \quad \text{and} \quad (p_1 p_3 - p_2^2) > 0 \tag{58}$$

Thus, one needs to determine the conditions that need to be imposed on γ, q_σ, and q_ξ such that $p_1 + p_3$ has the same sign as that of Λ and $p_1 p_3 - p_2^2 > 0$. The values of q_ξ that occur as the roots of Λ give the clue that if, for the given value of $\gamma > 0$, the following conditions are satisfied:

$$f_3 > 0, \qquad f_1 f_3 - f_2^2 < 0 \tag{59}$$

then $\mathbf{P}(\boldsymbol{x})$ remains positive for the choices

$$0 < q_\sigma(\boldsymbol{x}) < q_\sigma^{\text{cr}}(\boldsymbol{x}) \tag{60}$$

$$0 < q_\xi(\boldsymbol{x}) < q_\xi^{\text{cr}}(\boldsymbol{x}) \tag{61}$$

where

$$q_\sigma^{\text{cr}}(\boldsymbol{x}) = f_3 a^2/(f_2^2 - f_1 f_3) \tag{62}$$

$$q_\xi^{\text{cr}}(\boldsymbol{x}) = \frac{(f_3 a^2 - q_\sigma f_2^2 + f_1 f_3 q_\sigma)(2f_2^2 - f_1 f_3 + 2f_2\sqrt{f_2^2 - f_1 f_3})}{f_3^2(f_2^2 - f_1 f_3)} \tag{63}$$

Note that q_σ^{cr} and q_ξ^{cr} are continuous in the states σ and ξ. The conditions in Eq. (59) along with the criteria on the weights in Eqs. (62, 63) also guarantee that $\mathbf{P}(\boldsymbol{x})$ remains finite.

The domain over which $\mathbf{P}(\boldsymbol{x})$ remains positive-definite is denoted by

$$\mathcal{D}_{\mathbf{P}^+} = \{\boldsymbol{x}\text{: } \mathbf{P}(\boldsymbol{x}) \text{ is positive definite}\} \tag{64}$$

Given an engagement geometry and a value of the parameter $\gamma > 0$, where the state vector $\boldsymbol{x} \in D_{\text{SDC}}$, proposed SDRE-based solution exists corresponding to the SDC form of Eq. (7) if the state weights q_σ and q_ξ satisfy the conditions in Eqs. (62) and (63), respectively, and the engagement geometry satisfies the conditions in Eq. (59).

D. Derived Guidance Law

The impact-angle-constrained guidance law for the interceptor, which will be henceforth referred to as SDRE-IACDGGL and denoted by the subscript SDI, is computed according to Eq. (15) and has the following form:

$$u_{\text{SDI}} = G_1 \sigma + G_2 \xi \tag{65}$$

where

$$G_1 = \frac{\cos(\alpha - \theta) p_1}{r\Lambda} - \frac{p_2}{V_I \Lambda} \tag{66}$$

$$G_2 = \frac{\cos(\alpha - \theta) p_2}{r\Lambda} - \frac{p_3}{V_I \Lambda} \tag{67}$$

with p_1, p_2, p_3, and Λ being given by Eq. (57).

The domain where the guidance law can be applied while complying with all the constraints is

$$\mathcal{D}_{\text{SDI}} = \mathcal{D}_{\text{SDC}} \cap \mathcal{D}_{\mathbf{P}^+} \tag{68}$$

where $\mathcal{D}_{\text{SDC}}$ and $D_{\mathbf{P}^+}$ are shown in Eqs. (49) and (64), respectively.

In a neighborhood $\Omega \subseteq \mathcal{D}_{\text{SDI}}$ about the origin, local asymptotic stability is obtained where the conditions discussed in Theorem 3 are satisfied.

IV. Simulation Results

Performance of the guidance law derived in Sec. III.D is validated here by means of simulation. The guidance law is derived assuming ideal autopilots for both the interceptor and the target. However, autopilots with first-order dynamics are considered for both the interceptor and the target for simulation study. The simulations are carried out for two kinds of interceptor models: 1) a constant-speed interceptor model, and 2) a thrust-driven realistic interceptor model. The derived guidance law is tested on both the interceptor models against different kinds of target maneuver.

It is assumed here that α, V_I, θ can be measured, and the quantities β, V_T, $\dot{\theta}$ are available from estimation. The time constants of the interceptor's autopilot and the target's autopilot are denoted by τ_I and τ_T, respectively. Interceptor's autopilot output is denoted by a_I, and target's autopilot output is denoted by a_T. Acceleration due to gravity is denoted by g, which has a value of 10 m/s^2. Initial flight-path angles of the interceptor and the target are denoted by α_0 and β_0, respectively. The performance of SDRE-IACDGGL is compared to that of LQDG-CTIA. The LQDG-CTIA-based guidance law that is used here for comparison purpose has been described in the Appendix for the sake of completion. In an engagement scenario, guidance commands for SDRE-IACDGGL and LQDG-CTIA are computed considering the same value of the parameter γ. The argument $\boldsymbol{x}$ is dropped from q_σ and q_ζ for brevity. Note that the engagement trajectories are plotted by stretching the y axis for clarity.

A. Constant-Speed Interceptor and Target

The equations of motion of the interceptor are as follows:

$$\dot{x}_I = V_I \sin\alpha \tag{69a}$$

$$\dot{z}_I = V_I \cos\alpha \tag{69b}$$

$$\dot{\alpha} = a_I/V_I \tag{69c}$$

$$\dot{a}_I = (u - a_I)/\tau_I \tag{69d}$$

where (x_I, z_I) is the (x, z) coordinates of the interceptor.

The equations of motion of the target are as follows:

$$\dot{x}_T = -V_T \sin\beta \tag{70a}$$

$$\dot{z}_T = V_T \cos\beta \tag{70b}$$

Table 1 Initial engagement scenarios for nonmaneuvering target case

Entity	x, m	z, m	V, m/s
	Scenario 1/2		
Interceptor	0	0	600
Target	2,500	0	400
	Scenario 3		
Interceptor	0	0	600
Target	10,000	0	400

$$\dot{\beta} = a_T/V_T \tag{70c}$$

$$\dot{a}_T = (v - a_T)/\tau_T \tag{70d}$$

where (x_T, z_T) is the (x, z) coordinates of the target.

Interceptor and target speeds are considered to remain constant throughout the engagement period and are considered to be $V_I = 600$ m/s and $V_T = 400$ m/s, respectively. The autopilot time constants are $\tau_I = 0.1$ s and $\tau_T = 0.1$ s.

1. Nonmaneuvering Target

Though the guidance law is derived to intercept a maneuvering target at a given impact angle, it should exhibit its capability against nonmaneuvering targets as well. Three test scenarios are considered that exhibit the efficacy of SDRE-IACDGGL.

Scenario 1: An initial geometry with a high heading error is considered. The initial conditions for scenario 1 are shown in Table 1. Initial FPA of the interceptor and the target are $\alpha_0 = 70$ deg and $\beta_0 = 0$ deg, respectively. The interceptor is supposed to hit the nonmaneuvering target head on. The weights on the the states are $q_\sigma = 10^5$ and $q_\xi = q_\xi^{\text{cr}}/2$, respectively. Both the guidance laws SDRE-IACDGGL and LQDG-CTIA do not use the information that the target is nonmaneuvering, which is reflected by selection of a small value of 7 for the parameter γ. SDRE-IACDGGL misses the target by a distance less than 1 m and an impact-angle error less than 1 deg. But LQDG-CTIA misses the target by more than 1450 m. The engagement trajectories are shown in Fig. 2a. The acceleration profiles in Fig. 2b show that LQDG-CTIA has failed to produce the required lateral acceleration to obtain the required curvature in its trajectory. PTIA profiles resulting from these guidance laws are shown in Fig. 2c.

Scenario 2: LQDG-CTIA fails in scenario 1 because the chosen value of the parameter γ is smaller than the value of γ_∞, which has a value of 8.3 in this case. The expression of γ_∞ is given in Eq. (A8) in the Appendix. If γ is chosen to have a value greater than that of γ_∞, then LQDG-CTIA also produces satisfactory results. The same scenario given in scenario 1 is simulated with $\gamma = 8.5$ to check how LQDG-CTIA performs with a higher value of γ. In this case, both SDRE-IACDGGL and LQDG-CTIA yield a miss distance less than 1 m and an impact-angle error less than 1 deg. Figures 3a–3c show the engagement trajectories, guidance command, and PTIA, respectively.

Scenario 3: Here, the performance of SDRE-IACDGGL is compared to that of LQDG-CTIA in a scenario with a longer initial range. The initial engagement scenario is shown in Table 1. Initial FPA of the interceptor and the target are $\alpha_0 = 70$ deg and $\beta_0 = 0$ deg, respectively. The weights on the the states are $q_\sigma = 10^5$ and $q_\xi = q_\xi^{\text{cr}}/2$, respectively. With $\gamma = 7$, SDRE-IACDGGL imposes a miss distance less than 1 m and an error in impact angle less than 1 deg, whereas LQDG-CTIA fails to produce enough acceleration to hit this distant target and misses it by more than 5000 m. Both the scenarios have been simulated with a saturation level of $50g$ imposed on guidance command. Figures 4a–4c show the engagement trajectories, guidance command, and PTIA, respectively.

These results show that SDRE-IACDGGL performs well even for low values of γ.

2. Step Maneuver by Target

In this case, the target is assumed to execute a step maneuver with a magnitude of $5g$, and $\eta^C = 0$ deg. The interceptor and the target start

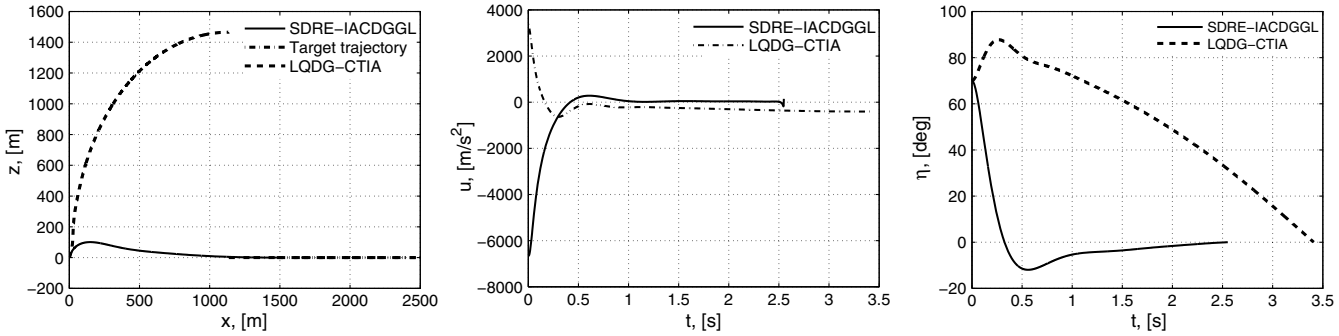

a) Engagement trajectory **b) Lateral acceleration of the interceptor** **c) Projected terminal impact angle**

Fig. 2 Engagement scenario for nonmaneuvering target (scenario 1).

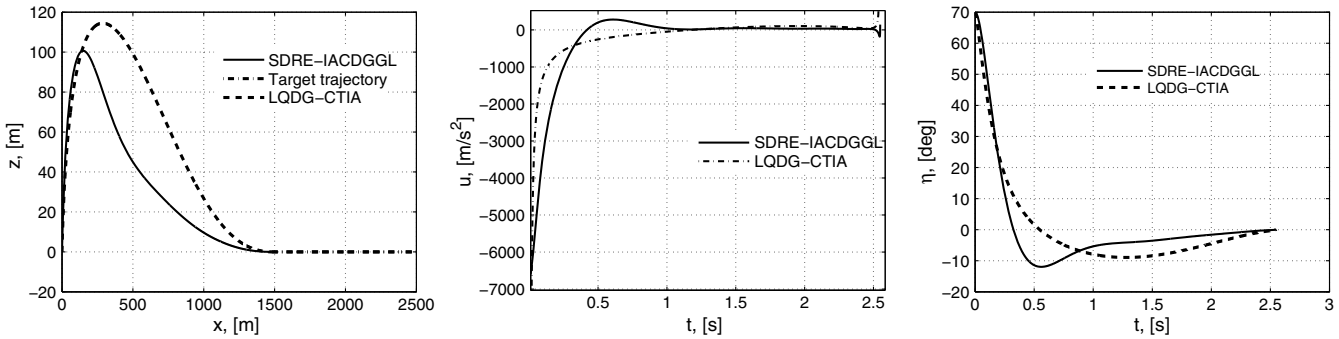

a) Engagement trajectory **b) Lateral acceleration of the interceptor** **c) Projected terminal impact angle**

Fig. 3 Engagement scenario for nonmaneuvering target (scenario 2).

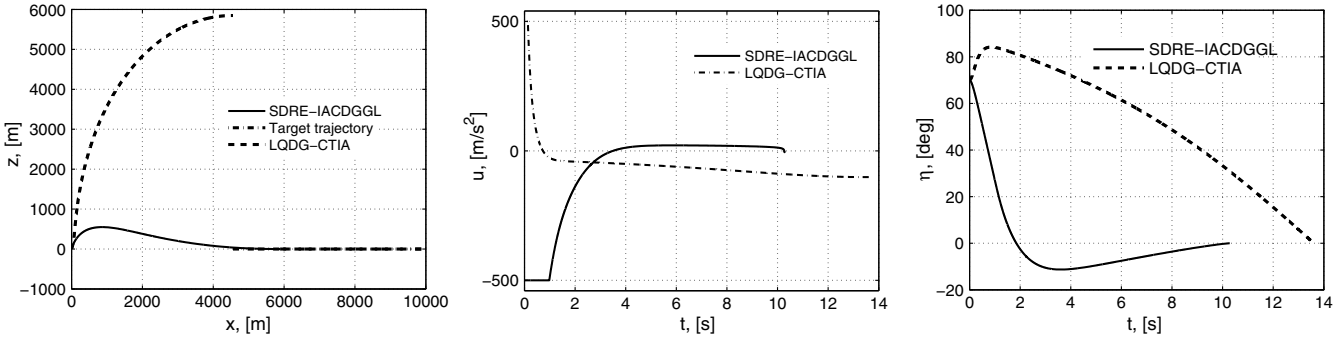

a) Engagement trajectory **b) Lateral acceleration of the interceptor** **c) Projected terminal impact angle**

Fig. 4 Engagement scenario for nonmaneuvering target (scenario 3).

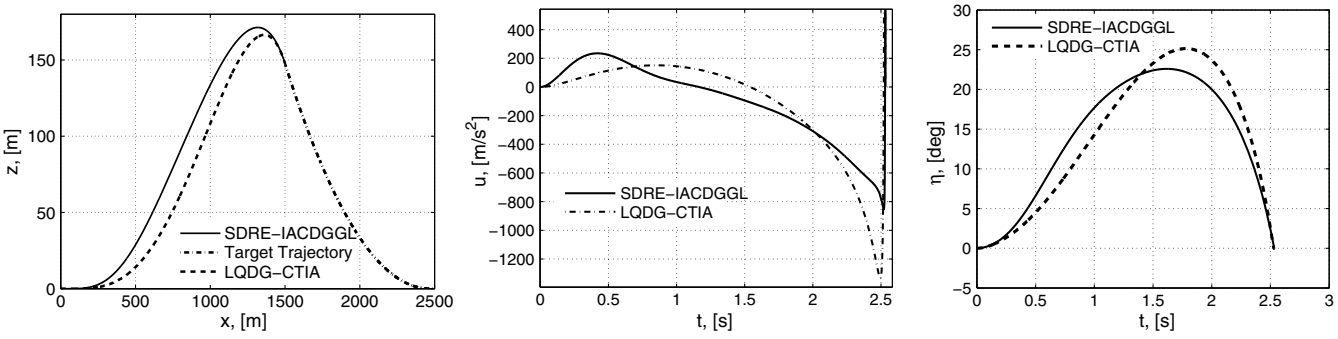

a) Engagement trajectory **b) Lateral acceleration of the interceptor** **c) Projected terminal impact angle**

Fig. 5 Engagement scenario with no guidance command saturation: target executes step maneuver.

from the initial conditions given in Table 1 for scenario 1, with $\alpha_0 = 0$ deg and $\beta_0 = 0$ deg, respectively. SDRE-IACDGGL yields a miss distance less than 1 m and an error in impact angle less than 1 deg with $q_\sigma = 10^5$, $q_\xi = q_\xi^{\text{cr}}/1.5$, and $\gamma = 7$. LQDG-CTIA guidance law also produces results with an equivalent accuracy. But with a saturation limit of $45g$ on guidance command, the miss distance and error in impact angle obtained by employing SDRE-IACDGGL (≈2.8 m and ≈3 deg, respectively) are smaller than those obtained by employing LQDG-CTIA guidance law (≈8 m and ≈7.8 deg, respectively). The engagement trajectories as well as the lateral acceleration of the interceptor and PTIA profiles for no saturation and with saturation on the interceptor's guidance command have been plotted in Figs. 5 and 6, respectively.

3. *Square-Wave Maneuver by Target*

Two engagement scenarios are considered here with $\eta^C = 0$ deg. In the first scenario, the target is considered to execute a square-wave maneuver with a magnitude of $5g$, time period of 3 s, and phase of 0 deg. The interceptor and the target start on a collision course from the initial conditions given in Table 1 for scenario 1, with $\alpha_0 = 0$ deg and $\beta_0 = 0$ deg, respectively. With the choice of the weights $q_\sigma = 10^5$, $q_\xi = q_\xi^{\text{cr}}/3$, and $\gamma = 8.5$, SDRE-IACDGGL yields a miss distance less than 1 m and an impact-angle error less than 1 deg. LQDG-CTIA guidance law yields a miss distance less than 1 m and an impact-angle error of ≈1.7 deg. With a saturation level of $42g$ on guidance command, SDRE-IACDGGL yields a miss distance of ≈1 m and an impact-angle error of ≈2.3 deg. On the other hand, LQDG-CTIA yields a miss distance of ≈2 m and impact-angle error of ≈11 deg. The engagement trajectories as well as the lateral acceleration of the interceptor and PTIA profiles for no saturation and with saturation on the guidance command have been plotted in Figs. 7 and 8, respectively.

In the second scenario, the interceptor and the target start from the initial conditions given in Table 1 for scenario 1, with $\alpha_0 = 70$ deg and $\beta_0 = 0$ deg, respectively. The target is considered to execute a square-wave maneuver with a magnitude of $5g$, time period of 1 s, and phase of 0 deg. SDRE-IACDGGL, with $q_\sigma = 10^5$, $q_\xi = q_\xi^{\text{cr}}/2$, and $\gamma = 8.5$, yields a miss distance less than 1 m and an impact-angle error of ≈3 deg. LQDG-CTIA guidance law also yields a miss distance less than 1 m, but the impact-angle error is ≈10 deg. With a

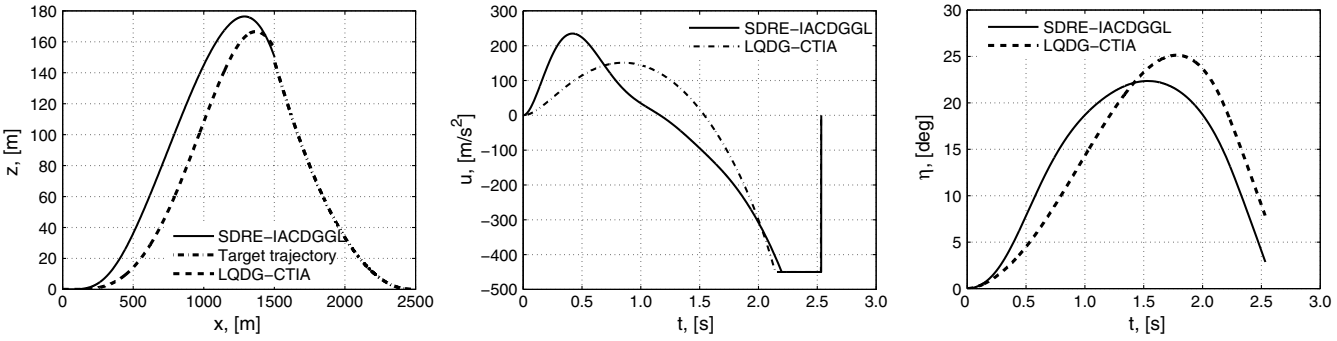

a) Engagement trajectory **b) Lateral acceleration of the interceptor** **c) Projected terminal impact angle**

Fig. 6 Engagement scenario with guidance command saturation: step maneuver by target.

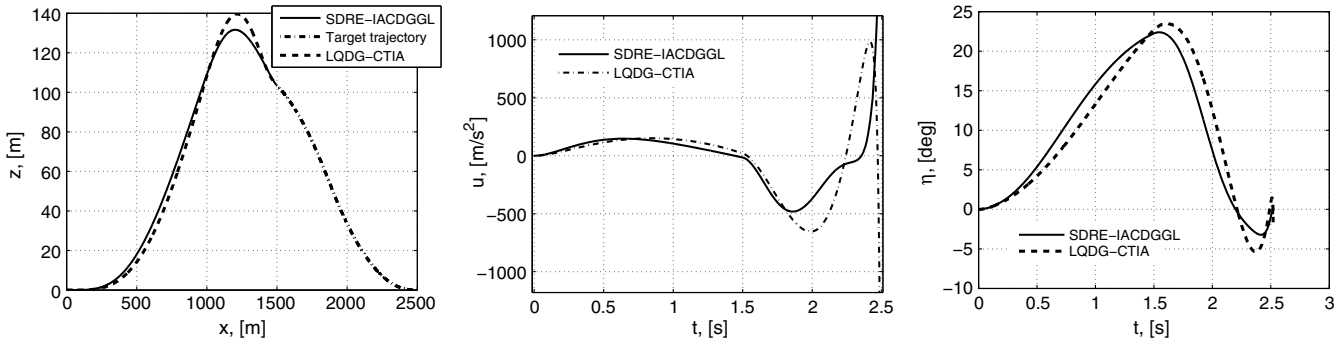

a) Engagement trajectory **b) Lateral acceleration of the interceptor** **c) Projected terminal impact angle**

Fig. 7 Engagement scenario with no guidance command saturation: target executes square-wave maneuver.

saturation level of $70g$ on the interceptor's guidance command, SDRE-IACDGGL yields a miss distance ≈1.5 m and impact-angle error of ≈5 deg. LQDG-CTIA also produces an equivalent result with a miss distance less than 2 m and an impact-angle error of ≈5 deg. The engagement trajectories as well as the lateral acceleration of the interceptor and PTIA profiles for no-saturation and with saturation on the interceptor's guidance command have been plotted in Figs. 9 and 10, respectively. Note that, in Fig. 9, the lateral acceleration shows wiggles because there is no saturation. These wiggles are at a very high value of lateral acceleration and are automatically killed due to saturation in Fig. 10.

B. Realistic Interceptor Model and Constant-Speed Target

In practical scenarios, the speed of the interceptor may not remain constant throughout the engagement period. Moreover, there will be influence of drag. To take such factors into account, in this section, a thrust-driven realistic interceptor model is considered. The target is considered to have constant speed and the same model as given by Eq. (70). The equations of motion of the interceptor are as follows:

$$\dot{x}_I = V_I \cos\alpha \tag{71}$$

$$\dot{z}_I = V_I \sin\alpha \tag{72}$$

$$\dot{V}_I = \frac{T_I - D}{m_I} - g\sin\alpha \tag{73}$$

$$\dot{\alpha} = \frac{a_I - g\cos\alpha}{V_I} \tag{74}$$

$$\dot{a}_I = \frac{u - a_I}{\tau_I} \tag{75}$$

The interceptor's autopilot time constant is $\tau_I = 0.1$ s.

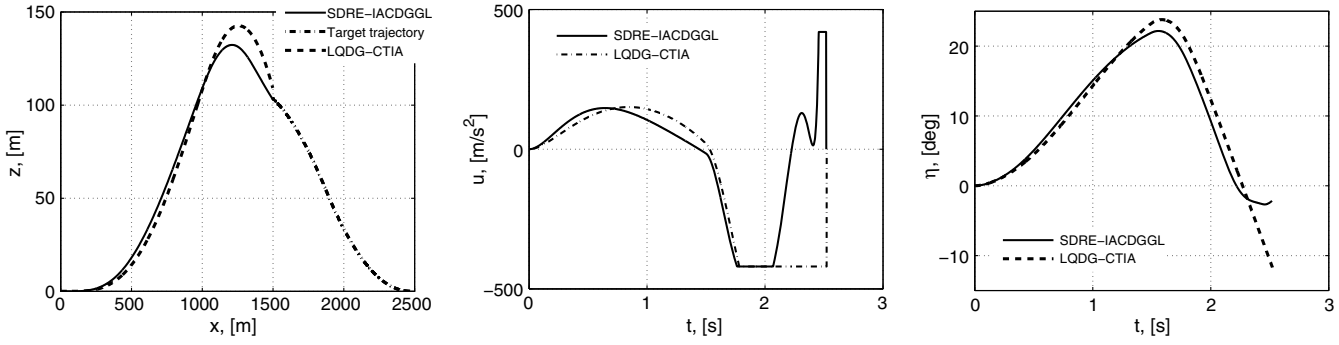

a) Engagement trajectory **b) Lateral acceleration of the interceptor** **c) Projected terminal impact angle**

Fig. 8 Engagement scenario with guidance command saturation: square-wave maneuver by target.

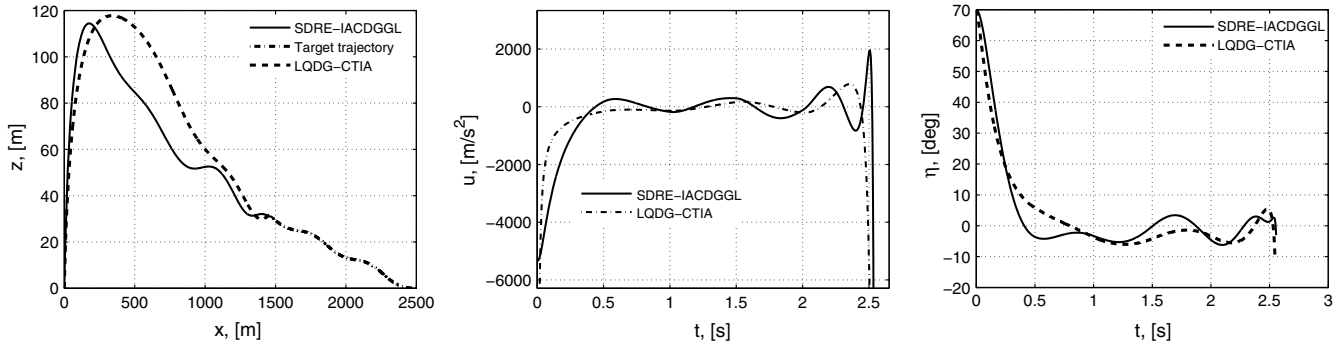

a) Engagement trajectory **b) Lateral acceleration of the interceptor** **c) Projected terminal impact angle**

Fig. 9 Engagement scenario: initial high heading error case.

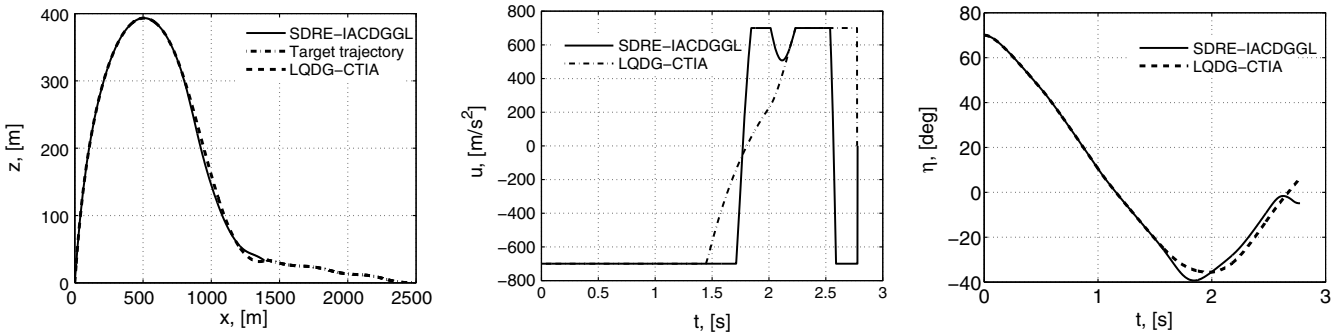

a) Engagement trajectory **b) Lateral acceleration of the interceptor** **c) Projected terminal impact angle**

Fig. 10 Engagement scenario: initial high heading error case. Guidance command saturated.

The aerodynamic drag acting on the interceptor is modeled as

$$D = D_0 + D_i \tag{76}$$

$$D_0 = C_{d0}\bar{Q}s \tag{77}$$

$$D_i = \frac{Ka_I^2 m_I^2}{\bar{Q}s} \tag{78}$$

$$K = \frac{1}{\pi A_r e} \tag{79}$$

$$\bar{Q} = \frac{1}{2}\rho V_I^2 \tag{80}$$

where C_{d0} is the zero-lift drag coefficient, K is the induced drag coefficient, A_r is the aspect ratio, e is the efficiency factor, ρ is the atmosphere density, s is the reference area, and $\bar{Q}$ is the dynamic pressure.

The aerodynamic model and properties are taken from [53]. The zero-lift drag coefficient and the induced drag coefficient are given next:

$$C_{d0} = \begin{cases} 0.02 & M < 0.93 \\ 0.02 + 0.2(M - 0.93) & 0.93 \le M < 1.03 \\ 0.04 + 0.06(M - 1.03) & 1.03 \le M < 1.1 \\ 0.0442 - 0.007(M - 1.1) & M \ge 1.1 \end{cases} \tag{81}$$

and

$$K = \begin{cases} 0.02 & M < 1.15 \\ 0.02 + 0.245(M - 1.15) & M \ge 1.15 \end{cases} \tag{82}$$

where M is the Mach number. The Mach number M has the following expression:

$$M = \frac{V_I}{\sqrt{1.4RT}}, \qquad R = 288 \tag{83}$$

where variation of temperature T with altitude z_I is related as

$$T = \begin{cases} 288.16 - 0.0065 z_I & z_I \le 11{,}000 \text{ m} \\ 216.66 & z_I \ge 11{,}000 \text{ m} \end{cases} \tag{84}$$

T has the unit of Kelvins.

The reference area s, used in Eq. (78), is assumed to be 1 m^2, and the thrust profile and mass of the vehicle are given by

$$T_I = \begin{cases} 33{,}000 \text{ N} & 0 \le t < 1.5 \text{ s} \\ 7500 \text{ N} & 1.5 \text{ s} \le t < 8.5 \text{ s} \\ 0 \text{ N} & t \ge 12 \text{ s} \end{cases} \tag{85}$$

and

$$m_I = \begin{cases} 135 - 14.53t \text{ kg} & 0 \le t < 1.5 \text{ s} \\ 113.205 - 3.331t \text{ kg} & 1.5 \text{ s} \le t < 8.5 \text{ s} \\ 90.035 \text{ kg} & t \ge 8.5 \text{ s} \end{cases} \tag{86}$$

The atmospheric density is given by

$$\rho(z_I) = 1.15579 - 1.058 \times 10^{-4} z_I + 3.725 \times 10^{-9} z_I^2 - 6.0 \times 10^{-14} z_I^3, \qquad z_I \in [0, 20000 \text{ m}] \tag{87}$$

1. Step Maneuver by Target

Scenario 1: The interceptor has to impose a terminal impact angle of 0 deg to a target that executes a maneuver with a constant magnitude of $5g$. Engagement geometries at the initial instant, and at the instant of closing the guidance loop, at $t_G = 1.5$ s, are shown in Table 2.

SDRE-IACDGGL yields a miss distance less than 1 m and an error in impact angle less than 1 deg, with $q_\sigma = 10^5$, $q_\xi = q_\xi^{\text{cr}}/1.5$, and $\gamma = 7$. LQDG-CTIA also yields an equivalent performance. Performances of both the guidance laws are tested with a saturation level on the interceptor's guidance command. With a saturation limit of $65g$ on guidance command, miss distance is ≈2.7 m and error in impact angle is less than 1.5 deg for SDRRE-IACDGGL. Miss distance obtained by employing LQDG-CTIA is ≈2 m, and error in impact angle is less than 1.5 deg in this case. The engagement trajectories, guidance command of the interceptor, PTIA, and the interceptor's velocity profiles for no-saturation and with saturation on the interceptor's guidance command have been plotted in Figs. 11 and 12, respectively. The velocity profiles of the interceptor, plotted in Figs. 11d and 12d, do not show any significant difference.

Scenario 2: The interceptor has to impose a terminal impact angle of 0 deg to a target that executes a maneuver with a constant magnitude of $3g$. Engagement geometries at the beginning and closing of the guidance loop, at $t_G = 1.5$ s, are shown in Table 3.

SDRE-IACDGGL yields a miss distance less than 1 m and an error in impact angle less than 1 deg with $q_\sigma = 10^5$, $q_\xi = q_\xi^{\text{cr}}/2$, and $\gamma = 7$. LQDG-CTIA also yields an equivalent performance.

Table 2 Scenario 1: realistic interceptor model considered (target executes step maneuver)

t, s	Entity	x, m	z, m	V, m/s	FPA, deg
0	Interceptor	0	0	600	10
0	Target	5000	0	400	0
1.5	Interceptor	1099	180.95	879.6	8.84
1.5	Target	4402.9	49.125	400	10.03

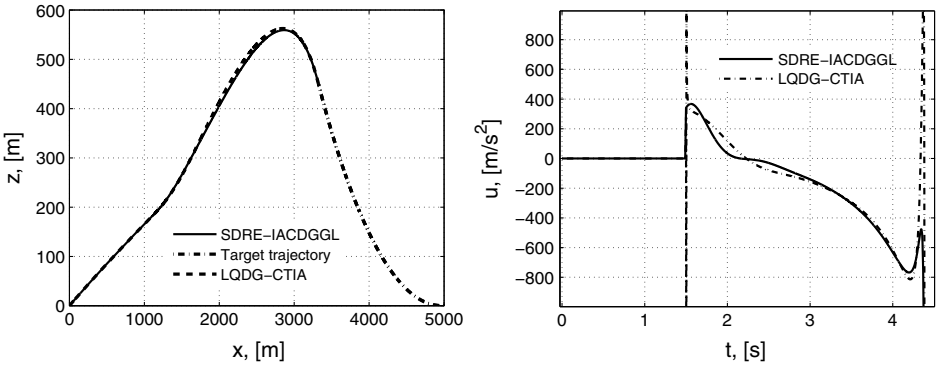

a) Engagement trajectory

b) Lateral acceleration of the interceptor

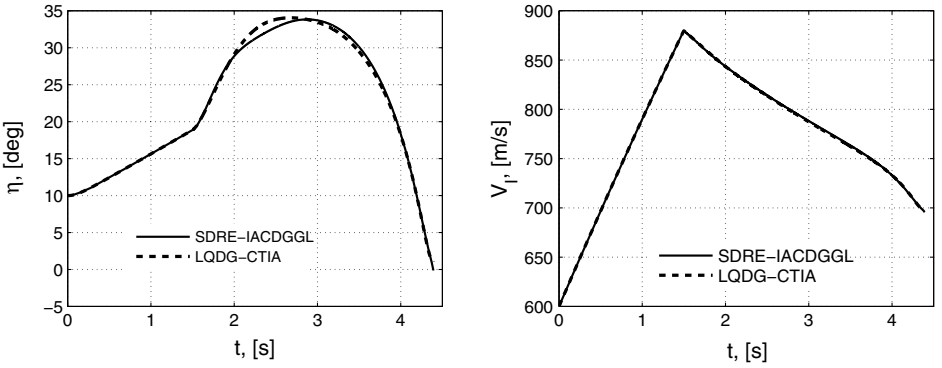

c) Projected terminal impact angle

d) Interceptor velocity

Fig. 11 Scenario 1: realistic interceptor, no saturation on guidance command. Target executes step maneuver.

Performances of both the guidance laws are tested with a saturation level on the interceptor's guidance command. With a guidance command saturation of $30g$, miss distance is $\approx$1.5 m and error in impact angle is $\approx$1 deg for SDRE-IACDGGL. LQDG-CTIA yields a miss distance of $\approx$7 m but an impact-angle error less than 1 deg. The engagement trajectories as well as lateral acceleration of the interceptor and PTIA profiles for no-saturation and with saturation of the interceptor guidance command have been plotted in Figs. 13 and 14, respectively. In this case, velocity profiles of the interceptor, plotted in Figs. 13d and 14d, do not show any significant difference.

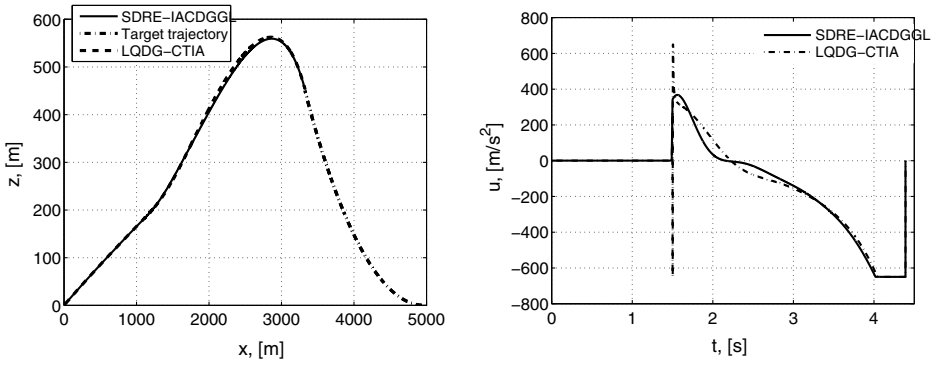

a) Engagement trajectory

b) Lateral acceleration of the interceptor

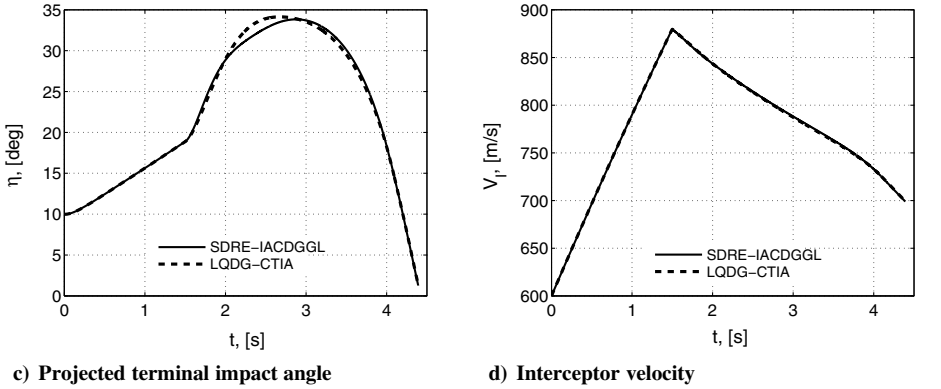

c) Projected terminal impact angle

d) Interceptor velocity

Fig. 12 Scenario 1: realistic interceptor, guidance command saturated. Target executes step maneuver.

Table 3 Scenario 2: realistic interceptor model considered (target executes step maneuver)

t, s	Entity	x, m	z, m	V, m/s	FPA, deg
0	Interceptor	0	0	600	30
0	Target	10,000	4,000	400	−45
1.5	Interceptor	968.16	546.1	877.85	≈29
1.5	Target	9555.6	3597.3	400	≈ − 39

2. Square-Wave Maneuver by Target

Scenario 1: In this case, the target executes a square-wave maneuver with a magnitude of $5g$ and time period of 2.25 s. The interceptor has to impose a terminal impact angle of 0 deg. The engagement geometries at the start of the engagement, and at the time of closing the guidance loop, at $t_G = 1.5$ s, are shown in Table 4. SDRE-IACDGGL in this case yields a miss distance less than 1 m and

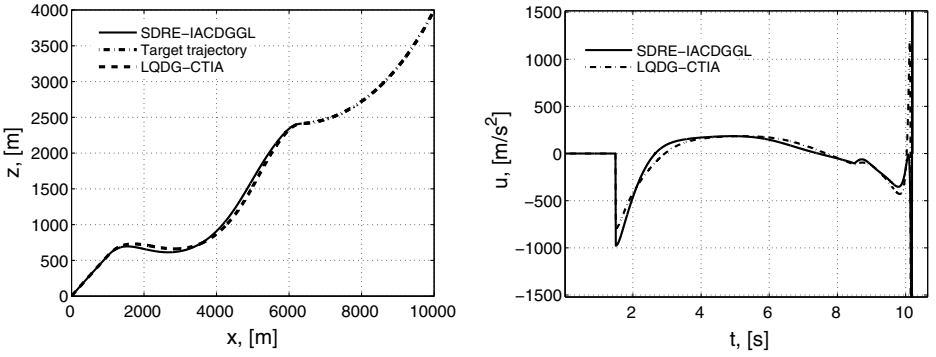

a) Engagement trajectory b) Lateral acceleration of the interceptor

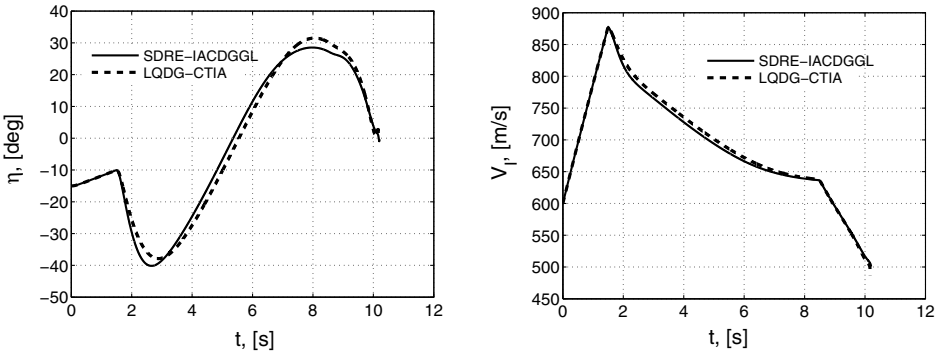

c) Projected terminal impact angle d) Interceptor velocity

Fig. 13 Scenario 2: realistic interceptor, no saturation on guidance command. Target executes step maneuver.

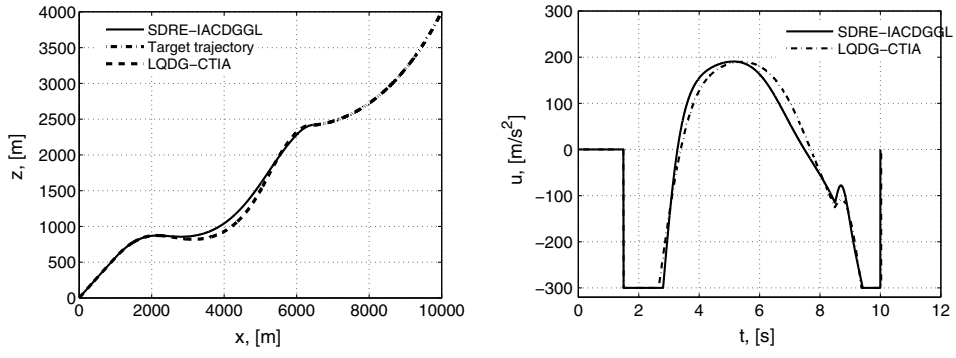

a) Engagement trajectory b) Lateral acceleration of the interceptor

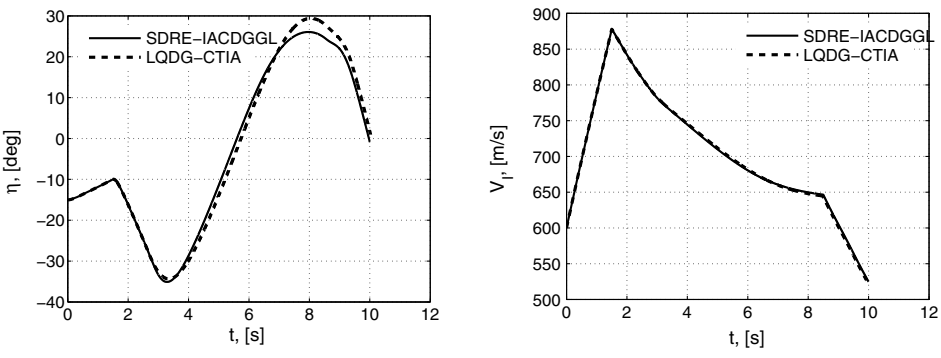

c) Projected terminal impact angle d) Interceptor velocity

Fig. 14 Scenario 2: realistic interceptor, guidance command saturated. Target executes step maneuver.

Table 4 Scenario 1: realistic interceptor model, square-wave maneuver by target

t, s	Entity	x, m	z, m	V, m/s	FPA, deg
0	Interceptor	0	0	600	10
0	Target	5000	0	400	0
1.5	Interceptor	1099	180.95	879.6	8.84
1.5	Target	4402.9	49.125	400	10.03

Table 5 Scenario 2: realistic interceptor model, square-wave maneuver by target

t, s	Entity	x, m	z, m	V, m/s	FPA, deg
0	Interceptor	0	0	600	30
0	Target	10000	4000	400	−45
1.5	Interceptor	968.16	546.1	877.85	≈29
1.5	Target	9543	3612.5	400	≈ − 35

an error in impact angle less than 1 deg with $q_\sigma = 10^5$, $q_\xi = q_\xi^{\rm cr}/3$, $\gamma = 7$. LQDG-CTIA also yields an equivalent performance with miss distance of ≈1 m and impact-angle error of ≈1 deg. With a saturation limit of $40g$, SDRE-IACDGGL yields a miss distance less than 1 m and an error of ≈2 deg in impact angle. On the other hand, LQDG-CTIA misses the target by ≈3.5 m with an impact-angle error of ≈12 deg. The engagement trajectories, lateral acceleration of the interceptor PTIA profiles, and interceptor's velocity profiles for no-saturation and with saturation of the interceptor's guidance command have been plotted in Figs. 15 and 16, respectively. Figures 15d and 16d show that, in the saturation and no-saturation cases, respectively, the velocity of the interceptor drops by ≈37 m/s and ≈11 m/s for LQDG-CTIA relative to that of SDRE-IACDGGL in the terminal phase.

Scenario 2: In this case, the target executes a square-wave maneuver with a magnitude of $5g$ and time period of 10 s. The engagement conditions are shown in Table 5 for the initial instant and the instant of closing the guidance loop at $t_G = 1.5$ s. The interceptor has to impose a terminal impact angle of 0 deg. SDRE-IACDGGL in this case yields a miss distance less than 1 m, but the error in impact angle is ≈7 deg, with $q_\sigma = 10^5$, $q_\xi = q_\xi^{\rm cr}/2$, $\gamma = 7$. LQDG-CTIA also yields a miss distance less than 1 m and impact-angle error of ≈6.5 deg. With a saturation limit of $50g$, SDRE-IACDGGL yields a miss distance of ≈5.5 m and an error in impact angle less than 1 deg. LQDG-CTIA yields a miss distance of ≈10 m and an error in impact angle of ≈2.7 deg. The engagement trajectories as well as lateral acceleration of the interceptor and PTIA profiles for no-saturation and with saturation of the interceptor's guidance command have been plotted in Figs. 17 and 18, respectively. Note that, Fig. 17d shows that the interceptor's velocity drops by ≈50 m/s at the terminal phase for SDRE-IACDGGL with respect to that of LQDG-CTIA. However, under saturation, significant difference in the interceptor's velocity profiles is not observed in Fig. 18d.

3. *Interception at Different Angle Specifications*

Next, the ability of the guidance law to intercept a maneuvering target at different specified impact angles is verified. The target is assumed to maneuver with a constant lateral acceleration of $5g$. The initial engagement geometry is considered to be the same as given in Table 2. In all the cases, $q_\sigma = 10^5$, $q_\xi = q_\xi^{\rm cr}/2$, and $\gamma = 7$.

Three different specifications of impact angle, $\eta^C \in \{-30, 45, 75 \text{ deg}\}$, are considered. Figures 19a–19c show the trajectories of the engagements, lateral acceleration profiles of the interceptor, and projected terminal impact angle over the engagement duration, respectively. At the time of closing the guidance loop at $t_G = 1.5$ s, the engagement scenario is the same for all the cases as shown in Table 2. The miss distances were less than 2 m, and terminal impact angles were within error a margin of 2.5 deg of the specified angle in all the cases.

Because the magnitudes of demanded accelerations are quite high, a saturation level of $100g$ is imposed on the guidance command, and the same scenarios are simulated. Figures 20a–20c show the trajectories of the engagements, lateral acceleration profiles of the interceptor, and projected terminal impact-angle profiles over the

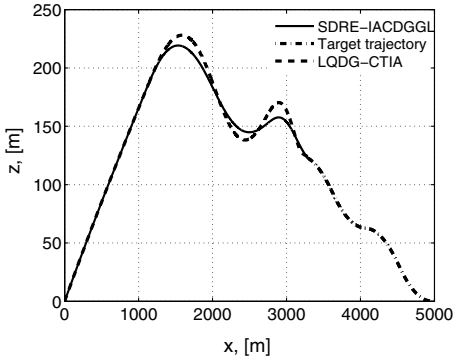

a) Engagement trajectory

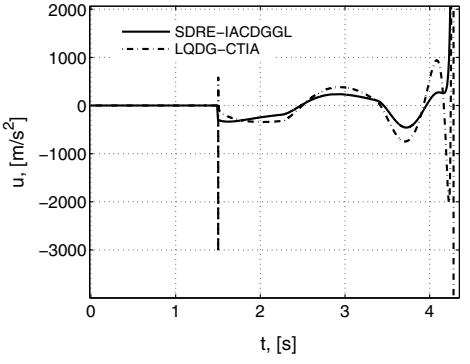

b) Lateral acceleration of the interceptor

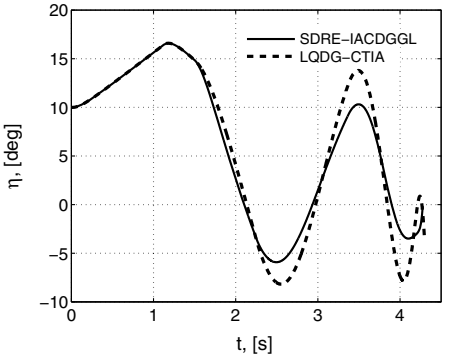

c) Projected terminal impact angle

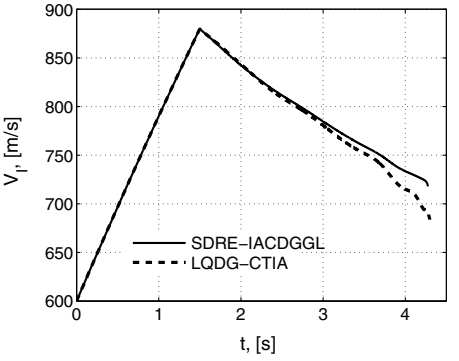

d) Interceptor velocity

Fig. 15 Scenario 1: realistic interceptor, no saturation on guidance command. Square-wave maneuver by target.

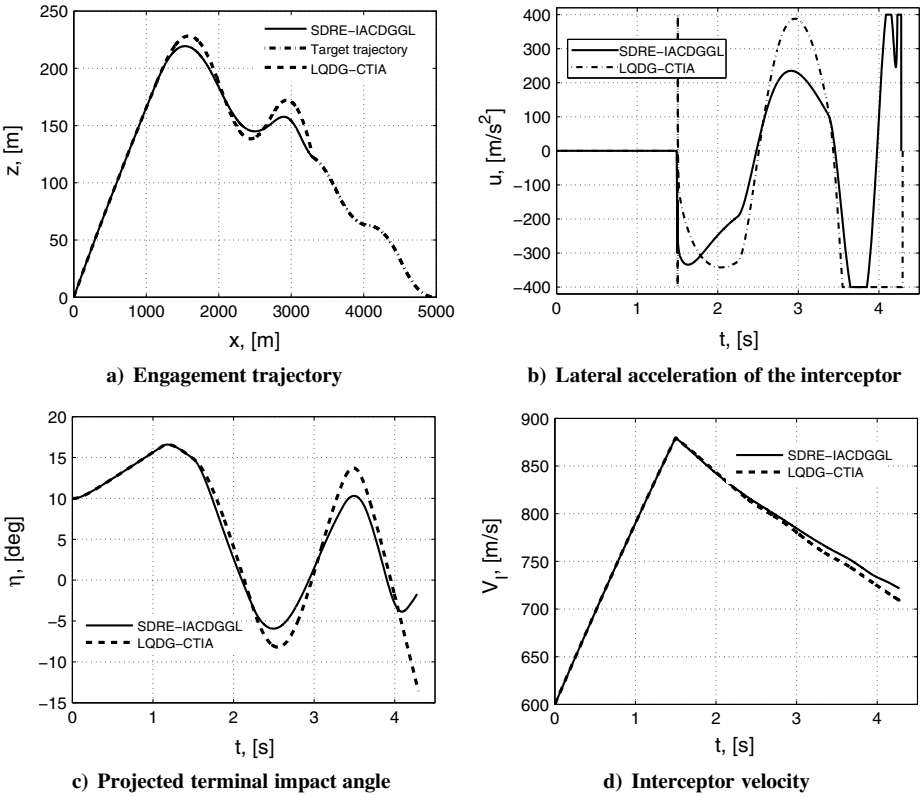

a) Engagement trajectory

b) Lateral acceleration of the interceptor

c) Projected terminal impact angle

d) Interceptor velocity

Fig. 16 Scenario 1: Realistic interceptor, guidance command saturated. Square-wave maneuver by target.

engagement duration, respectively. The error in impact angle is ≈3 deg for $\eta^C = -30$ deg, but this error quantity remains within 1 deg when $\eta^C \in \{45, 75 \text{ deg}\}$. For $\eta^C = -30$ deg, miss distances is ≈4 m, whereas it is less than 1 m for $\eta^C \in \{45, 75 \text{ deg}\}$.

It is observed that the greater the shaping of curvature of the required trajectory is, which is governed by the specified impact angle and maneuver of the target, the greater the magnitude of the peak acceleration demand is. To achieve interception of the target at the specified impact angle, at a fair precision level, the interceptor should have adequate maneuverability advantage over the target such that it can exert sufficient acceleration to rectify its path.

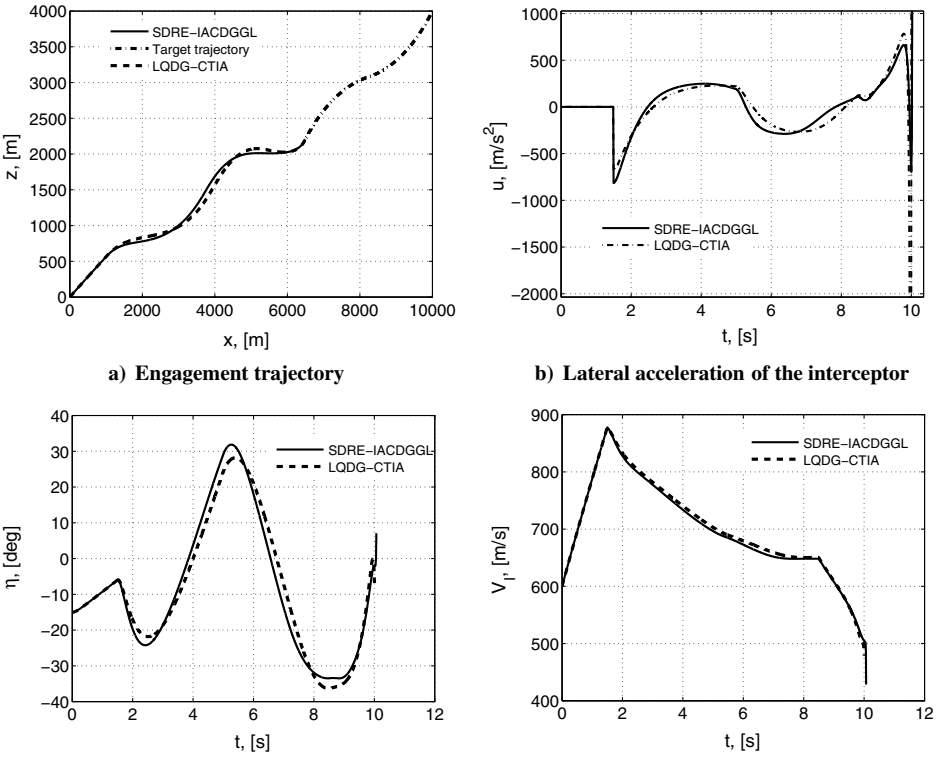

a) Engagement trajectory

b) Lateral acceleration of the interceptor

c) Projected terminal impact angle

d) Projected terminal impact angle

Fig. 17 Scenario 2: Realistic interceptor, no saturation on guidance command. Square-wave maneuver by target.

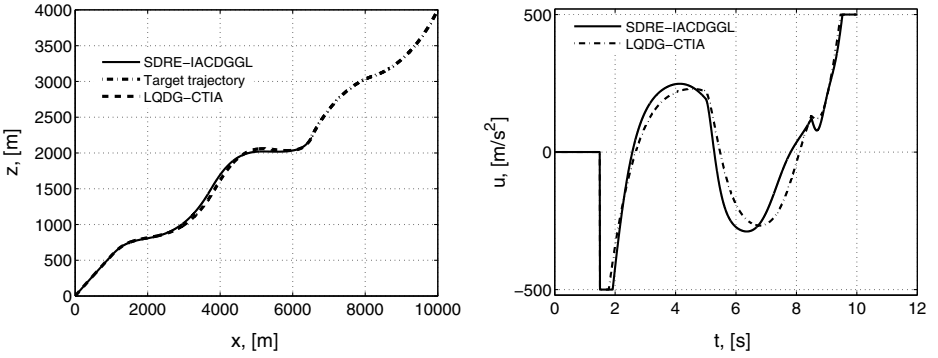

a) Engagement trajectory b) Lateral acceleration of the interceptor

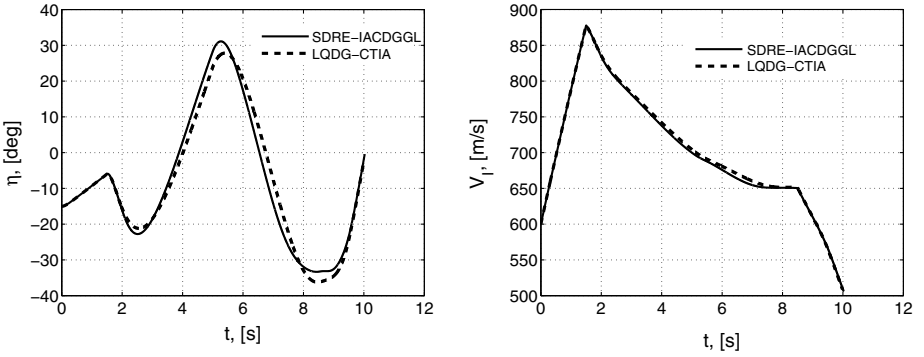

c) Projected terminal impact angle d) Projected terminal impact angle

Fig. 18 Scenario 2: Realistic interceptor, guidance command saturated. Square-wave maneuver by target.

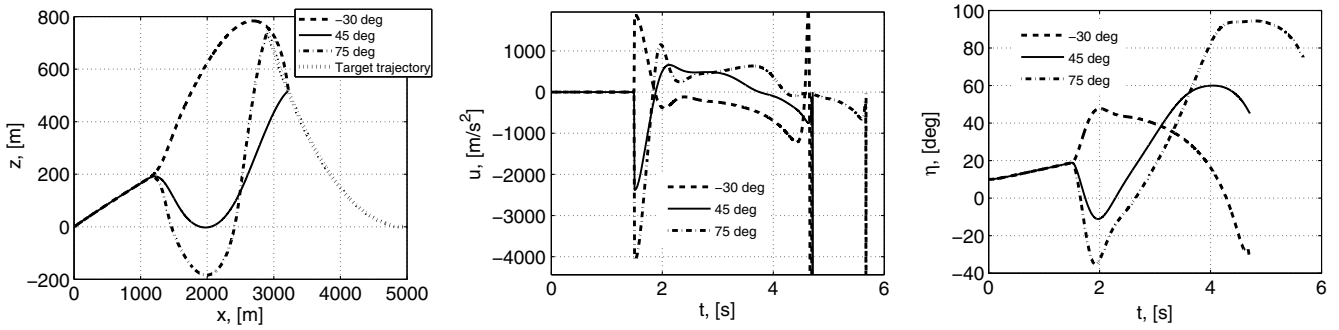

a) Engagement trajectory b) Lateral acceleration of the interceptor c) Projected terminal impact angle

Fig. 19 Interception at different impact angles: realistic interceptor model, no guidance command saturation.

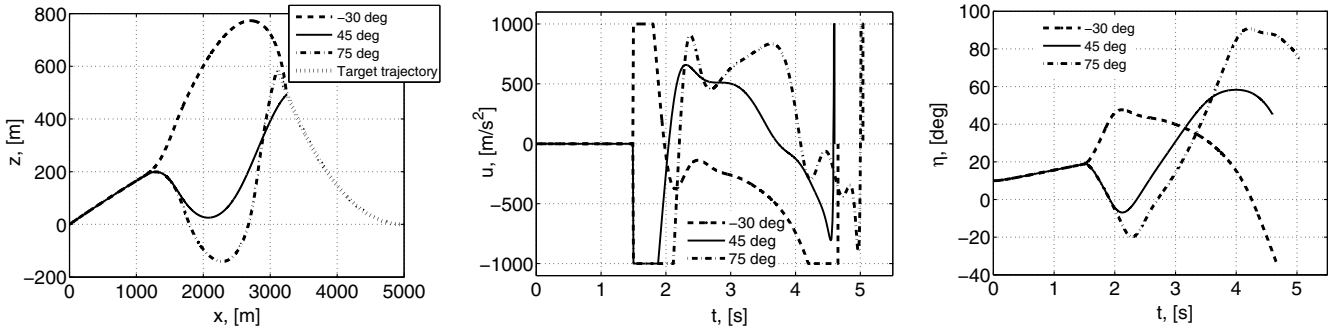

a) Engagement trajectory b) Lateral acceleration of the interceptor c) Projected terminal impact angle

Fig. 20 Interception at different impact angles: realistic interceptor, guidance command saturated.

V. Conclusions

A closed-form guidance law based on nonlinear differential games theory that allows an interceptor to impose a prespecified impact angle on interception of a maneuvering target has been presented in this paper. The state-dependent Riccati equation method based solution presented here for nonlinear zero-sum differential games takes care of the target's maneuver as well as the nonlinear nature of the state equations in the impact-angle-constrained guidance

problem. Conditions are studied for local asymptotic stability of the closed-loop system when the target does not maneuver and for the case when it employs a worst-case strategy. In simulation study, the proposed guidance law is found to achieve small values of miss distance and impact-angle error against targets with different maneuver profiles if an interceptor is fortified with large maneuver advantage over a target. With suitable choice of the weights, the guidance law derived in this paper performs quite well and excels over the linear quadratic differential games-based constrained terminal impact-angle guidance law in those cases where initial engagement geometries have large deviations from the collision courses. Performance of the proposed guidance law is also tested using a realistic interceptor model in simulation. Performance of the derived guidance law is not vulnerable to unpredictability of a target's maneuver. Implementation of the derived guidance law does not depend on time-to-go estimate explicitly. An interesting study would be to investigate if the proposed method can be further refined to obtain a solution more close to the optimal one and ensures global asymptotic stability even in the presence of the target's maneuver. Another direction of study might be to consider the aerodynamic model of the interceptor and analytically derive the guidance law using the technique presented in this paper.

Appendix: Linear Quadratic Differential Games

In [17], LQDG was derived, assuming integral cost on $u_\perp^2$ and $v_\perp^2$, where $u_\perp$ and $v_\perp$ are the components of the lateral acceleration vector of the interceptor and the target, respectively, perpendicular to the LOS. Howevr, note that the objective function used in this work to derive the SDRE-based guidance law includes integral cost on u^2 and v^2. Therefore, for comparative study, an equivalent derivation of the LQDG-CTIA that includes integral cost on u^2 and v^2 is used here. As it has been derived in [17], the equivalent guidance law for the interceptor takes the following form:

$$u = N_1 Z_1/\hat{t}_{\rm go}^2 + N_2 V_I Z_2/\hat{t}_{\rm go} \tag{A1}$$

where

$$N_1 = \frac{6\gamma^2(-k_I\gamma^2 V_T^2 + 2k_I V_I^2 + k_T V_I V_T)}{\Delta_{LQDGCTIA}^{\infty}} \tag{A2}$$

$$N_2 = -\frac{2\gamma^2 V_T(V_T\gamma^2 k_I^2 + 3V_I k_I k_T + 2V_T k_T^2)}{\Delta_{LQDGCTIA}^{\infty}} \tag{A3}$$

$$\Delta_{LQDGCTIA}^{\infty} = -\gamma^4 k_I^2 V_T^2 + 4\gamma^2 k_I^2 V_I^2 + 6\gamma^2 k_I k_T V_I V_T + 4\gamma^2 k_T^2 V_T^2 - k_T^2 V_I^2 \tag{A4}$$

which is obtained from the following objective functional:

$$J = \frac{q_{ZEM}}{2} Z_1^2(t_f) + \frac{q_{ZEAE}}{2} Z_2^2(t_f) + \frac{1}{2}\int_{t_0}^{t_f} (u^2 - \gamma^2 v^2)\,{\rm d}t \tag{A5}$$

by setting $q_{ZEM} \to \infty$ and $q_{ZEAE} \to \infty$. These weights emphasize on perfect interception and zero error in terminal impact angle, respectively. The terms k_I and k_T correspond to $(\alpha - \theta)$ and $(\beta + \theta)$ at t_0, respectively. The states Z_1 and Z_2 are zero-effort miss distance and zero-effort angle error, respectively, which are given by the following expressions:

$$Z_1 = -V_r \hat{t}_{\rm go}^2 \sigma, \qquad Z_2 = \alpha + \beta - \eta^C \tag{A6}$$

Time-to-go $\hat{t}_{\rm go}$ is estimated as

$$\hat{t}_{\rm go} = -r/V_r \tag{A7}$$

The greatest positive root of $\Delta_{LQDGCTIA}^{\infty}$ is designated by γ_∞. It has the following expression:

$$\gamma_\infty = (k_I V_I + k_T V_T + (k_I^2 V_I^2 + k_I k_T V_I V_T + k_T^2 V_T^2)^{1/2})/(k_I V_T) \tag{A8}$$

A conjugate point does not exist if the value of the parameter γ is greater than γ_∞.

Acknowledgments

The authors would like to thank A. Ratnoo and S. Ghosh for their valuable suggestions.

References

[1] Ratnoo, A., and Ghose, D., "Impact Angle Constrained Interception of Stationary Targets," *Journal of Guidance, Control, and Dynamics*, Vol. 31, No. 6, 2008, pp. 1817–1822. doi:10.2514/1.37864

[2] Ratnoo, A., and Ghose, D., "Impact Angle Constrained Guidance Against Nonstationary Nonmaneuvering Targets," *Journal of Guidance, Control, and Dynamics*, Vol. 33, No. 1, 2010, pp. 269–275. doi:10.2514/1.45026

[3] Lee, C. H., Kim, T. H., and Tahk, M. J., "Interception Angle Control Guidance Using Proportional Navigation with Error Feedback," *Journal of Guidance, Control, and Dynamics*, Vol. 36, No. 5, 2013, pp. 1556–1561. doi:10.2514/1.58454

[4] Kim, B. S., Lee, J. G., and Han, H. S., "Biased PNG Law for Impact with Angular Constraint," *IEEE Transactions on Aerospace and Electronic Systems*, Vol. 34, No. 1, 1998, pp. 277–288. doi:10.1109/7.640285

[5] Erer, K. S., and Merttopçuoğlu, O., "Indirect Impact-Angle-Control Against Stationary Targets Using Biased Pure Proportional Navigation," *Journal of Guidance, Control, and Dynamics*, Vol. 35, No. 2, 2012, pp. 700–704. doi:10.2514/1.52105

[6] Kim, T. H., Park, B. G., and Tahk, M. J., "Bias-Shaping Method for Biased Proportional Navigation with Terminal-Angle Constraint," *Journal of Guidance, Control, and Dynamics*, Vol. 36, No. 6, 2013, pp. 1810–1816. doi:10.2514/1.59252

[7] Lu, P., Doman, D. B., and Schierman, J. D., "Adaptive Terminal Guidance for Hypervelocity Impact in Specified Direction," *Journal of Guidance, Control, and Dynamics*, Vol. 29, No. 2, 2006, pp. 269–278. doi:10.2514/1.14367

[8] Sun, M., Xu, Q., Du, S., Chen, Z., and Zhang, D., "Practical Solution to Impact Angle Control in Vertical Plane," *Journal of Guidance, Control, and Dynamics*, Vol. 37, No. 3, 2014, pp. 1022–1027. doi:10.2514/1.61792.

[9] Manchester, I., and Savkin, A. V., "Circular Navigation Missile Guidance with Incomplete Information and Uncertain Autopilot Model," *Journal of Guidance, Control, and Dynamics*, Vol. 27, No. 6, 2004, pp. 1078–1083. doi:10.2514/1.3371

[10] Kim, M., and Grider, K., "Terminal Guidance for Impact Attitude Angle Constrained Flight Trajectories," *IEEE Transactions on Aerospace and Electronic Systems*, Vol. 9, No. 6, 1973, pp. 852–859. doi:10.1109/TAES.1973.309659

[11] Song, T. L., Shin, S. J., and Cho, H., "Impact Angle Control for Planar Engagements," *IEEE Transactions on Aerospace and Electronic Systems*, Vol. 35, No. 4, 1999, pp. 1439–1444. doi:10.1109/7.805460

[12] Ryoo, C. K., Cho, H., and Tahk, M. J., "Optimal Guidance Laws with Terminal Impact Angle Constraint," *Journal of Guidance, Control, and Dynamics*, Vol. 28, No. 4, 2005, pp. 724–732. doi:10.2514/1.8392

[13] Ryoo, C. K., Cho, H., and Tahk, M., "Time-to-Go Weighted Optimal Guidance with Impact Angle Constraints," *IEEE Transactions on Control Systems Technology*, Vol. 14, No. 3, 2006, pp. 483–492. doi:10.1109/TCST.2006.872525

[14] Ohlmeyer, E. J., and Phillips, C. A., "Generalized Vector Explicit Guidance," *Journal of Guidance, Control, and Dynamics*, Vol. 29, No. 2, 2006, pp. 261–268. doi:10.2514/1.14956.

[15] Lee, Y. I., Kim, S. H., Lee, J. I., and Tahk, M. J., "Analytic Solutions of Generalized Impact-Angle-Control Guidance Law for First-Order Lag System," *Journal of Guidance, Control, and Dynamics*, Vol. 36, No. 1, 2013, pp. 96–112. doi:10.2514/1.57454

[16] Idan, M., Golan, O., and Guelman, M., "Optimal Planar Interception with Terminal Constraints," *Journal of Guidance, Control, and Dynamics*, Vol. 18, No. 6, 1995, pp. 1273–1279. doi:10.2514/3.21541

[17] Shaferman, V., and Shima, T., "Linear Quadratic Guidance Laws for Imposing a Terminal Intercept Angle," *Journal of Guidance, Control, and Dynamics*, Vol. 31, No. 5, 2008, pp. 1400–1412. doi:10.2514/1.32836

[18] Taub, I., and Shima, T., "Intercept Angle Missile Guidance Under Time Varying Acceleration Bounds," *Journal of Guidance, Control, and Dynamics*, Vol. 36, No. 3, 2013, pp. 686–699. doi:10.2514/1.59139

[19] Cho, H., Ryoo, C. K., Tsourdos, A., and White, B., "Optimal Impact Angle Control Guidance Law Based on Linearization About Collision Triangle," *Journal of Guidance, Control, and Dynamics*, Vol. 37, No. 3, 2014, pp. 958–964. doi:10.2514/1.62910

[20] Nesline, F. W., and Zarchan, P., "New Look at Classical vs Modern Homing Missile Guidance," *Journal of Guidance, Control, and Dynamics*, Vol. 4, No. 1, 1981, pp. 78–85. doi:10.2514/3.56054

[21] Ben-Asher, J., and Yaesh, I., *Advances in Missile Guidance Theory*, Vol. 180, Progress in Astronautics and Aeronautics, AIAA, Reston, VA, 1998, pp. 127–140, Chap. 5.

[22] Lukacs, J. A., and Yakimenko, O. A., "Trajectory-Shaping Guidance for Interception of Ballistic Missiles During the Boost Phase," *Journal of Guidance, Control, and Dynamics*, Vol. 31, No. 5, 2008, pp. 1524–1531. doi:10.2514/1.32262

[23] Ratnoo, A., and Ghose, D., "State-Dependent Riccati-Equation-Based Guidance Law for Impact-Angle-Constrained Trajectories," *Journal of Guidance, Control, and Dynamics*, Vol. 32, No. 1, 2009, pp. 320–326. doi:10.2514/1.37876

[24] Arita, S., and Ueno, S., "Optimal Feedback Guidance for Nonlinear Missile Model with Impact Time and Angle Constraints," *AIAA Guidance, Navigation, and Control (GNC) Conference*, AIAA Paper 2013-4785, 2013. doi:10.2514/6.2013-4785

[25] Ghose, D., Dam, B., and Prasad, U. R., "A Spread Acceleration Guidance Scheme for Command Guided Surface-to-Air Missiles," *Proceedings of the IEEE National Aerospace and Electronics Conference*, IEEE Publ., Piscataway, NJ, May 1989, pp. 202–208. doi:10.1109/NAECON.1989.40214

[26] Dwivedi, P. N., Bhattacharya, A., and Padhi, R., "Suboptimal Midcourse Guidance of Interceptors for High Speed Targets with Alignment Angle Constraint," *Journal of Guidance, Control, and Dynamics*, Vol. 34, No. 3, 2011, pp. 860–877. doi:10.2514/1.50821

[27] Oza, H. B., and Padhi, R., "Impact-Angle-Constrained Suboptimal Model Predictive Static Programming Guidance of Air-to-Ground Missiles," *Journal of Guidance, Control, and Dynamics*, Vol. 35, No. 1, 2012, pp. 153–164. doi:10.2514/1.53647

[28] Maity, A., Oza, H. B., and Padhi, R., "Generalized Model Predictive Static Programming and Angle-Constrained Guidance of Air-to-Ground Missiles," *Journal of Guidance, Control, and Dynamics*, Vol. 37, No. 6, 2014, pp. 1897–1913. doi:10.2514/1.G000038

[29] Indig, N., Ben-Asher, J. Z., and Farber, N., "Near-Optimal Spatial Midcourse Guidance Law with an Angular Constraint," *Journal of Guidance, Control, and Dynamics*, Vol. 37, No. 1, 2014, pp. 214–223. doi:10.2514/1.60356

[30] Shima, T., "Intercept-Angle Guidance," *Journal of Guidance, Control, and Dynamics*, Vol. 34, No. 2, 2011, pp. 484–492. doi:10.2514/1.51026

[31] Kumar, S. R., Rao, S., and Ghose, D., "Sliding-Mode Guidance and Control for All-Aspect Interceptors with Terminal Angle Constraints," *Journal of Guidance, Control, and Dynamics*, Vol. 35, No. 4, 2012, pp. 1230–1246. doi:10.2514/1.55242

[32] Kumar, S. R., Rao, S., and Ghose, D., "Nonsingular Terminal Sliding Mode Guidance with Impact Angle Constraints," *Journal of Guidance, Control, and Dynamics*, Vol. 37, No. 4, 2014, pp. 1114–1130. doi:10.2514/1.62737

[33] Wang, X., and Wang, J., "Partial Integrated Guidance and Control for Missiles with Three-Dimensional Impact Angle Constraints," *Journal of Guidance, Control, and Dynamics*, Vol. 37, No. 2, 2014, pp. 644–657. doi:10.2514/1.60133

[34] Bardhan, R., and Ghose, D., "Intercepting Maneuvering Target with Specified Impact Angle by Modified SDRE Technique," *Proceedings of the IEEE American Control Conference*, IEEE Publ., Piscataway, NJ, June 2012, pp. 4613–4618. doi:10.1109/ACC.2012.6315507

[35] Feng, Y., Anderson, B. D. O., and Rotkowitz, M., "A Game Theoretic Algorithm to Compute Local Stabilizing Solutions to HJBI Equations in Nonlinear H_∞ Control," *Automatica*, Vol. 45, No. 4, 2009, pp. 881–888. doi:10.1016/j.automatica.2008.11.006

[36] Ammar, G., Basar, T., Bitmead, R., Bittanti, S., Callier, F. M., Colaneri, P., De Nicolao, G., Gevers, M., Kucera, V., Lancaster, P., Laub, A. J., Martin, C. F., Rodman, L., Shayman, M. A., Trentelman, H. L., Willems, J. L., and Willems, J. C., *The Riccati Equation*, edited by Bittanti, S., Laub, A. J., and Willems, J. C., Vol. 338, Communications and Control Engineering Series, Springer–Verlag, Berlin, 1991, pp. 163–196, Chap. 7.

[37] Çimen, T., "Survey of State-Dependent Riccati Equation in Nonlinear Optimal Feedback Control Synthesis," *Journal of Guidance, Control, and Dynamics*, Vol. 35, No. 4, 2012, pp. 1025–1047. doi:10.2514/1.55821

[38] Cloutier, J. R., and Zipfel, P. H., "Hypersonic Guidance via the State-Dependent Riccati Equation Control Method," *Proceedings of the IEEE International Conference on Control Applications*, IEEE Publ., Piscataway, NJ, Aug. 1999, pp. 219–224. doi:10.1109/CCA.1999.806179

[39] Balakrishnan, S. N., and Xin, M., "Robust State Dependent Riccati Equation Based Guidance Laws," *Proceedings of the American Control Conference*, IEEE Publ., Piscataway, NJ, June 2001, pp. 3352–3357. doi:10.1109/ACC.2001.946146

[40] Vaddi, S., Menon, P. K., and Ohlmeyer, E. J., "Numerical State-Dependent Riccati Equation Approach for Missile Integrated Guidance Control," *Journal of Guidance, Control, and Dynamics*, Vol. 32, No. 2, pp. 699–703. doi:10.2514/1.34291

[41] Tyan, F., and Shen, J. F., "SDRE Missile Guidance Law," *Proceedings of the 8th IEEE International Conference on Control and Automation*, IEEE Publ., Piscataway, NJ, June 2010, pp. 866–870. doi:10.1109/ICCA.2010.5524364

[42] Xin, M., Balakrishnan, S. N., and Ohlmeyer, E. J., "Integrated Guidance and Control of Missiles with θ- D Method," *IEEE Transactions on Control Systems Technology*, Vol. 14, No. 6, 2006, pp. 981–992. doi:10.1109/TCST.2006.876903

[43] Ball, J., and Helton, J., "H_∞ Control for Nonlinear Plants: Connections with Differential Games," *Proceedings of the 28th Conference on Decision and Control*, IEEE Publ., Piscataway, NJ, Dec. 1989, pp. 956–962. doi:10.1109/CDC.1989.70268

[44] Cloutier, J. R., "State-Dependent Riccati Equation Techniques: An Overview," *Proceedings of the American Control Conference*, Vol. 2, IEEE Publ., Piscataway, NJ, 1997, pp. 932–936. doi:10.1109/ACC.1997.609663

[45] Friedland, B., *Advanced Control System Design*, Prentice–Hall, Upper Saddle River, NJ, 1996, pp. 110–112.

[46] Basar, T., and Olsder, G., *Dynamic Noncooperative Game Theory*, 2nd ed., Society for Industrial and Applied Mathematics, Philadelphia, 1999.

[47] van der Schaft, A. J., "On a State Space Approach to Nonlinear H∞ Control," *Systems and Control Letters*, Vol. 16, No. 1, 1991, pp. 1–8. doi:10.1016/0167-6911(91)90022-7

[48] Basar, T., and Bernhard, P., H_∞ *Optimal Control and Related Minimax Design Problems*, Birkhauser, Boston, 1991, Chap. 4.

[49] Cloutier, J. R., D'Souza, C. N., and Mracek, C. P., "Nonlinear Regulation and Nonlinear H_∞ Control via the State-Dependent Riccati Equation Technique: Part 1, Theory; Part 2, Examples," *Proceedings of the 1st International Conference on Nonlinear Problems in Aviation and Aerospace*, Embry-Riddle Aeronautical Univ. Press, Prescott, AZ, May 1996, pp. 117–141.

[50] Rawling, A. G., "On Nonzero Miss Distance," *Journal of Spacecraft and Rockets*, Vol. 6, No. 1, 1969, pp. 81–83. doi:10.2514/3.29539

[51] Doyle, J. C., Glover, K., Khargonekar, P. P., and Francis, B. A., "State-Space Solutions to Standard H_2 and H_∞ Control Problems," *IEEE Transactions on Automatic Control*, Vol. 34, No. 8, 1989, pp. 831–847. doi:10.1109/9.29425

[52] Menon, P. K., Lam, T., Crawford, L. S., and Cheng, V. H. L., "Real-Time Computational Methods for SDRE Nonlinear Control of Missiles," *Proceedings of the 2002 IEEE American Control Conference*, IEEE Publ., Piscataway, NJ, June 2002, pp. 232–237. doi:10.1109/ACC.2002.1024809

[53] Kee, P. E., Dong, L., and Siong, C. J., "Near Optimal Midcourse Guidance Law for Flight Vehicle," *36th AIAA Aerospace Sciences Meeting and Exhibit*, AIAA Paper 1998-0583, Jan. 1998, pp. 1–11.